SLAC-PUB-1004
LBL-572
(TH) and (EXP)
December 1971

A STUDY OF THE INCLUSIVE REACTION $\gamma p \rightarrow \pi^- +$ (ANYTHING) WITH POLARIZED PHOTONS AT 2.8, 4.7, AND 9.3 GeV*

K. C. Moffeit, J. Ballam, G. B. Chadwick, M. Della-Negra,** R. Gearhart,
J. J. Murray, P. Seyboth,*** C. K. Sinclair, I. O. Skillicorn****
H. Spitzer,† and G. Wolf ††

Stanford Linear Accelerator Center
Stanford University, Stanford, California 94305

H. H. Bingham, W. B. Fretter, W. J. Podolsky,††
M. S. Rabin, A. H. Rosenfeld, R. Windmolders ††† and G. P. Yost

Department of Physics and Lawrence Berkeley Laboratory
University of California, Berkeley, California 94720

and

R. H. Milburn
Tufts University, Medford, Mass. 02155

(A shorter version of this paper has been submitted to Phys. Rev.)

---

* Work supported in part by the U. S. Atomic Energy Commission and the National Science Foundation.

** On leave from College de France, Paris, France.

*** On leave from Max-Planck Institut für Physik und Astrophysik, Munich, Germany.

**** Present address: University of Glasgow, Dept. of Natural Philosophy, Glasgow, Scotland.

† On leave from University of Hamburg, Hamburg, Germany.

†† Present address: DESY, Hamburg, Germany

††† Present address: Laboratoire Interuniversitaire des Hautes Energies, Brussels, Belgium.

ABSTRACT

We study the inclusive spectra of π^- mesons from the events obtained in three exposures of the SLAC 82" HBC to a nearly monochromatic polarized photon beam of mean energies 2.8, 4.7, and 9.3 GeV. The data are presented in terms of transverse momentum $p_\perp$ and three suggested choices for the other independent variable, i.e., the longitudinal momentum $p_\parallel$ in the laboratory system, the rapidity variable $y = \frac{1}{2} \ln \left[(E+p_\parallel)/(E-p_\parallel)\right]$, and the variable suggested by Feynman $x = p^*_\parallel/p^*_{max}$ in the c.m.s. The 4π geometry of the bubble chamber allows us to cover the entire kinematically allowed range of these variables. We show that exact limiting fragmentation does not occur at our energies, but the data are compatible with an approach to a limiting distribution as $A + B s^{-1/2}$. The qualitative features of the structure function $f(x, p_\perp^2)$ in terms of Feynman's x-variable are similar at the three energies. Quantitatively, we find 5-10% differences between the 4.7 and 9.3 GeV data near $x=0$. We find $f(x, p_\perp^2)$ is not factorizable into independent functions of x and $p_\perp^2$. For our data the mean π^- multiplicity is described well by $\langle n^- \rangle = c^- \ln s + d^-$, where $c^- = 0.44 \pm 0.04$ and $d^- = 0.07 \pm 0.08$. Following the procedure suggested by Bali <u>et al.</u>, we calculate c^- from our experimentally observed 9.3 GeV structure function at $x=0$ and find $c^- = 0.44 \pm 0.02$ in agreement with the value obtained directly. We find a correlation between the azimuth of the π^- and the photon polarization plane only for $x > 0.3$ when elastic ρ^0 photoproduction is excluded. Lastly, we note that the distribution of π^- longitudinal momentum is not symmetric in the "quark frame" where $p_{Target} = 1.5\, p_{Beam}$.

INTRODUCTION

We present a study of the inclusive reaction

$$\gamma p \rightarrow \pi^- + \text{(anything)} \qquad (1)$$

at photon energies of 2.8, 4.7, and 9.3 GeV. Some data from a small exposure at 1.44 GeV are also given. The differential cross section for such a reaction can be written with the detected particle phase space explicitly shown:

$$d^3\sigma = \frac{d^3\vec{p}}{E} f_1(s, \vec{p}) \quad , \qquad (2)$$

where $\vec{p}$ and E are the momentum and energy of the pion and s is the center-of-mass energy squared. It has been suggested[1, 2, 3, 4] that the structure function, $f_1(s, \vec{p})$, when expressed in terms of an appropriate set of variables should have a simple form at large s. Three sets of variables have been proposed:

(i) Longitudinal momentum. Benecke et al.[1] have proposed the use of $p_{\parallel}$, the longitudinal momentum of the produced pion in the laboratory frame. At large s they suggest that $f_1(s, \vec{p})$ of Eq. (2) should be independent of s for small $p_{\parallel}$.

(ii) The rapidity variable. Feynman[2] has proposed the use of the variables $p_{\perp}$ and y, where $p_{\perp}$ is the transverse momentum of the pion and

$$y = \frac{1}{2} \ln \left[\frac{E + p_{\parallel}}{E - p_{\parallel}}\right] \qquad (3)$$

is the "rapidity". Here, the energy E and $p_{\parallel}$ are evaluated in the laboratory frame. After an integration over the azimuthal distribution of the π^-, Eq. (2) becomes simply

$$d^2\sigma = dy\, dp_{\perp}^2\, \pi f_2(s, y, p_{\perp}^2) \quad , \qquad (4)$$

i.e., the denominator E is incorporated into dy. The multiperipheral model predicts that in this set of variables, the structure function should have a simple form at large s; namely, that it becomes independent of s for y near its minimum and maximum values and that for central y values $f_2(s,y,p_\perp^2)$ is a function of $p_\perp^2$ only.[3,4]

(iii) Feynman x-variable. Feynman has suggested that the structure function of Eq. (2) "scales" at high energy. That is, as $s \to \infty$, it becomes a function only of $p_\perp^2$ and the ratio $x = p_\parallel^*/p_{max}^*$, where $p_\parallel^*$ is the c.m.s. longitudinal pion momentum and p_{max}^* is the maximum c.m.s. pion momentum.[5] The differential cross section, Eq. (2), in terms of these variables, becomes

$$d^2\sigma = \pi \frac{p_{max}^*}{E^*} dx\, dp_\perp^2 \quad f_3(x,p_\perp^2,s) , \tag{5}$$

where E* is the c.m.s. energy of the pion.

To illustrate the connection between the variables we give in Fig. 1 the relation between $p_\parallel$ in the laboratory and the variables x (Fig. 1a) and y (Fig. 1b) for our 9.3 GeV data. The upper boundary for $p_\parallel > 0$ in both cases corresponds to $p_\perp = 0$; points above the kinematic boundary in Fig. 1a are due to the finite width of the photon energy spectrum. The scatter plot of x and y shown in Fig. 1c displays how the region near x=0 is expanded when expressed in terms of y. The 4π-geometry of the bubble chamber allows us to cover the entire kinematically allowed range of these variables.

At high energies Vander Velde[6] has shown that an energy independent distribution in $f_1(p_\parallel,p_\perp^2)$ for target-fragmented pions results in a structure function $f_3(x,p_\perp^2)$ which is independent of s for the corresponding x-region. However, this equivalence is not valid for the photon energies used here.

In this paper we present our data in terms of the three sets of variables discussed above. We study the characteristics of the structure function in order to: a) determine if any of these sets of variables give a simple description, like that expected in the high energy region, at our moderate photon energies; b) determine the dependence of the structure function on these variables; c) investigate the dependence of the average pion multiplicity on s; and d) compare inclusive pion photoproduction with that from hadronic reactions.

EXPERIMENTAL PROCEDURES.

We have studied photoproduction of hadrons using a nearly monochromatic polarized photon beam at 2.8, 4.7, and 9.3 GeV in the 82" LBL-SLAC hydrogen bubble chamber. We have obtained 92, 150, and 138 events/μb at the three energies, respectively. Figure 2 shows the photon energy spectra at the three energies; the energy resolution is $\pm(3-4)\%$. The low energy tail of the spectrum gives $< 2.5\%$ of the π^- mesons produced. Furthermore, in the case of 3-constraint events (no outgoing neutrals), we fitted for E_γ and rejected low energy events.

We used all well measured 3, 5, 7, and 9-prong events; one-prong events do not have a negative track. Each topology was weighted separately for its fraction of unmeasurable events. There is a small contamination from unidentified K^- mesons which we estimate to be $0.5 \pm 0.5\%$ $(2 \pm 2\%)$ and $\langle 3 \pm 3\% \rangle$ at 2.8 (4.7) and $\langle 9.3 \rangle$ GeV, respectively. Events having an identified strange particle were not included in this study. The fractions of π^- mesons from these events are estimated to be $1.3 \pm 0.2\%$ $(2.9 \pm 0.2\%)$ and $\langle 4.3 \pm 0.2\% \rangle$ at 2.8 (4.7) and $\langle 9.3 \rangle$ GeV. We have not applied these two roughly compensating (in numbers) types of corrections to the distributions given in this paper unless otherwise stated.

All photographs were scanned at least twice, giving overall scanning losses of $\lesssim 1\%$. However, we found greater losses in the reaction $\gamma p \rightarrow \pi^+\pi^- p$ at small momentum transfers; in addition this reaction has some contamination from wide-angle e^+e^- pairs. All events giving an accepted fit to $\gamma p \rightarrow \pi^+\pi^- p$ were used in this study and a total correction to the channel $\gamma p \rightarrow \pi^+\pi^- p$ of -1±1, (+5±1), <+2±1>% at 2.8, (4.7), and <9.3> GeV is included in the results reported here. We estimate systematic uncertainties in the cross sections to be less than 3%.

CROSS SECTIONS

We show in Fig. 3 the total photoproduction cross section[7,8] versus the center-of-mass energy squared at our three energies; also shown are the results of a small exposure made at 1.44 GeV. Although the total cross section is approximately constant in this energy region, the topological cross sections as seen from Fig. 3 vary rapidly with energy. The cross sections for larger multiplicities increase with energy. A similar behavior is found in πp, Kp, and pp interactions.[9]

LONGITUDINAL MOMENTUM DISTRIBUTION IN THE LABORATORY

The hypothesis of limiting fragmentation put forward by Benecke _et al._[1] suggests that the spectra of low momentum particles become independent of the beam energy as the beam energy becomes large. To test if this hypothesis holds at our energies we give in Fig. 4

$$\mathscr{F}(p_{\parallel}) = \int_0^{\infty} \left(E \frac{d^2\sigma}{dp_{\perp}^2 dp_{\parallel}} \right) dp_{\perp}^2$$

in the laboratory frame for inclusive π^- production. The structure function rises rapidly from $p_{\parallel} < 0$ (backward production) to $p_{\parallel} \sim 500$ MeV followed by a more gradual fall off at high pion momenta. For small $p_{\parallel}$ (target fragmentation region) the curves are qualitatively the same; however, as seen in the insert of Fig. 4, the structure function at 9.3 GeV for $p_{\parallel} < 300$ MeV is lower by 10-30% (2 - 5 standard deviations at every point) than at 4.7 GeV. This means that in the laboratory system we do not observe exact limiting fragmentation in $\mathscr{F}(p_\parallel)$ at our energies.[10]

To further demonstrate the energy dependence we show in Fig. 5 the dependence of the structure function on the square of the transverse momentum, $p_\perp^2$, in the region near $p_\parallel$ (lab) = 0. Again, we find the 9.3 GeV data systematically lower than the 4.7 GeV results.

Mueller[11] has suggested that the single-particle distributions in the inclusive reaction $a + b \rightarrow c$ + (anything) can be related to the forward elastic three-body amplitude $a + b + \bar{c} \rightarrow a + b + \bar{c}$. Assuming that this amplitude is dominated by the usual Regge singularities, (i) the Pomeranchuk trajectory with $\alpha_p(0) = 1$ and (ii) the approximately exchange-degenerate meson trajectories (ρ, $P' = f$, ω, A_2) with $\alpha_M(0) \simeq 0.5$, Chan et al.[12] predict that the invariant cross section should reach a limiting distribution as $A + Bs^{-1/2}$ where A and B are independent of s. In order to test this prediction we give in Fig. 6 $\mathscr{F}(p_\parallel, s)$ for various intervals in $p_\parallel$ versus $s^{-1/2}$. Our data are consistent with the predicted $s^{-1/2}$ dependence.

Using the duality hypothesis, Chan et al.[12] also suggest that when the quantum numbers of the three-body system $a + b + \bar{c}$ are exotic a limiting distribution will be obtained at lower energies than if $a + b + \bar{c}$ were nonexotic. This means that reactions such as

$$p + p \rightarrow \pi^- + \text{(anything)}$$
$$K^+ + p \rightarrow \pi^- + \text{(anything)}$$
$$\pi^+ + p \rightarrow \pi^- + \text{(anything)}$$

which have exotic quantum numbers in $ab\bar{c}$ (i.e., $pp\pi^+$, $K^+p\pi^+$, $\pi^+p\pi^+$) will approach limiting behavior more rapidly than

$$\pi^- + p \rightarrow \pi^- + \text{(anything)}$$
$$\gamma + p \rightarrow \pi^- + \text{(anything)}$$

which are nonexotic (i.e., $\pi^-p\pi^+$ and $\gamma p\pi^+$).

To compare the pion spectra from photoproduction to those from hadron-induced reactions we normalize the distributions by dividing by the asymptotic total cross section of each reaction, as suggested by Chan et al.[12] Figure 7 shows

$$\frac{1}{\sigma_T(\infty)} \cdot \frac{d\sigma}{dp_{\parallel}}$$

in the laboratory frame for our 9.3 GeV photoproduction data together with the results of M.-S. Chen et al.[13,14] The normalized π^- cross sections from the "exotic" pp, K^+p and π^+p reactions agree but are a factor 2 smaller than the π^- cross sections from the "nonexotic" π^-p and γp reactions. We note that the π^- cross sections from photoproduction and the π^-p reaction are remarkably similar.

THE RAPIDITY VARIABLE

The introduction of the rapidity variable, y, results in the following simplifications for the structure function $f_2(s,y,p_\perp^2)$:

(a) The differential cross section is simply related to the structure function without a phase space factor,

$$d^2\sigma = dy\, dp_\perp^2\;\; \pi\; f_2(s,y,p_\perp^2) \quad .$$

(b) Under a Lorentz boost along the beam axis, y transforms into $y + \ln \gamma\,(1+\beta)$ where γ and β define the boost. Therefore, the form of the structure function is invariant under boost; it is only translated in y.

Arguing from two fundamental multiperipheral concepts, (a) that transverse momenta are limited and (b) that distant particles on the multiperipheral chain are uncorrelated, K. Wilson[3] and C. DeTar[4] predict that at sufficiently high incident energies, the function $f_2(y, p_\perp^2, s)$ has three characteristic features:

(i) An energy-independent limiting behavior of $f_2(y, p_\perp^2)$ is expected as the total energy is increased, for $(y - y_{min})$ or $(y_{max} - y)$ sufficiently small. This corresponds to limiting fragmentation of the target (region I of Fig. 8) and the beam particle (region III of Fig. 8), respectively.

(ii) Fragmentation of the target is independent of the beam particle, and vice versa.

(iii) The central region (labeled II in Fig. 8) of the spectrum is independent of both beam and target particles; it is independent of y and its width increases logarithmically with increasing energy.

At sufficiently high energy the above features also follow from Feynman's parton model.[2]

In Fig. 9 we show the scatter plot in y and $p_\perp^2$ at 9.3 GeV for the π^- of reaction (1). The boundaries imposed by the kinematical constraints at small and large y values are clearly visible. The points concentrate at small $p_\perp^2$ and at y near its central value. In Fig. 10 we show $d\sigma/dy$; in particular, no extended flat region is observed (region II of Fig. 8).[16] For the three energies we find roughly gaussian distributions in $d\sigma/dy$ whose width increases with increasing energy. Furthermore, we find in the target region (small y) a significant decrease in $d\sigma/dy$ with increasing photon energy (e.g., from Fig. 10 at $y = 0.5$ the 9.3 GeV value is $\sim 20\%$ lower than the 4.7 GeV result). We conclude that we do not have exact limiting target fragmentation at our energies. To test limiting fragmentation of the beam region we compare $d\sigma/dy$ at an equal distance from y_{max}. Figure 10 shows that $d\sigma/dy$ at $(y-y_{max})$ also decreases with increasing photon energy.

In Fig. 9 we saw clearly how the kinematic boundary narrows the range in y as transverse momentum increases. Thus, a flat distribution in

$$\frac{d^2\sigma}{dy\,dp_\perp^2}$$

will not result in a flat $d\sigma/dy$ when integrated over all transverse momenta. In Fig. 11 we give $d\sigma/dy$ for various intervals of transverse momenta. At 2.8 and 4.7 GeV no extended flat region is observed even when $p_\perp^2$ is restricted to a narrow interval; at 9.3 GeV the data are inconclusive.

The absence of a flat region in $d\sigma/dy$ would not be surprising at our energies in view of the following argument. We assume that the influence of the target fragmentation π^- is given by the kinematic region in which significant production of nucleon resonances at the nucleon vertex occurs. Nucleon resonance production occurs for masses up to 2 GeV corresponding to π^- laboratory momenta from the resonance decay up to ~ 1 GeV and hence to values of y up to 2.7. Therefore, the target fragmentation region can be expected to extend up to values of $y=2$ to 3. On the other hand we observe that ρ^0's which are elastically produced by fragmentation of the beam photons influence the y-distribution down to $y=2.5$ at 9.3 GeV. Hence, the beam and target fragmentation regions overlap to some extent at our energies. This may explain the apparent lack of a central plateau region.

FEYNMAN x-VARIABLE

In terms of variables $x=p_\parallel^*/p_{max}^*$ and $p_\perp^2$ we write the differential cross section as

$$d^2\sigma = \pi\,\frac{p_{max}^*}{E^*}\,dx\,dp_\perp^2\;\; f_3(x, p_\perp^2, s) \quad .$$

Feynman[2] has suggested that at high energies the structure function is independent of s, that is

$$f_3(x, p_\perp^2, s) \xrightarrow[s \to \infty]{} f_3(x, p_\perp^2) \quad .$$

In Fig. 12 we show the integrated structure function

$$F(x) = \frac{1}{\pi} \int_0^\infty \frac{E^*}{p^*_{max}} \frac{d^2\sigma}{dx dp_\perp^2} dp_\perp^2 \quad . \tag{6}$$

The same qualitative features hold at the three energies: a rapid increase from negative x to $x = 0$ by three orders of magnitude, a relatively flat region to $x \sim 0.6$, and a drop at large x (the narrow peak at large x is a reflection of the Δ^{++} production via $\gamma p \to \pi^- \Delta^{++}(1236)$ which falls off rapidly with increasing energy). We seem to see scaling to within ±10% over most of the x-region. To investigate this apparent scaling more carefully we display the energy dependence of the integrated structure function in Fig. 13, where F(x, s) is shown integrated over various x-intervals as a function of s. Although, there is a tendency for the rate of change of F(x, s) with respect to s to decrease, only measurements at higher energies will tell how close our 9.3 GeV data is to the scaling limit.

Figure 14 shows the comparison of the structure functions for different beam particles in terms of the x-variable. We again divide our 9.3 GeV data by $\sigma_{TOT}(\infty)$ and plot it together with similarly normalized $\pi^\pm$ data at 18 GeV/c of Shepard et al.[17] The region $x < 0.2$ corresponds to the interval in $p_\parallel$ given in Fig. 7. Again we find that the photoproduction structure function is similar to that of $\pi^- p$ but is larger than that of $\pi^+ p$. Not unexpectedly, the shapes of the distributions do not agree for $x > 0.2$, since the three reactions are initiated by different beam particles.

In the vector dominance model of photon interactions the reaction $\gamma p \rightarrow \rho^{0} p$ can be considered the analog of elastic scattering in hadron-induced reactions. In the following we shall investigate to what extent the exclusion of this quasi-elastic process affects the behavior of the structure function.

Because of the well known difficulties in separating ρ^{0} from background[7] we have attempted to eliminate the reaction $\gamma p \rightarrow \rho^{0} p$ by the simplest cut: we refer to all events of $\gamma p \rightarrow \pi^{+}\pi^{-} p$ with $M_{\pi^{+}\pi^{-}} < 1.0$ GeV as "elastic" ρ^{0} events.

In Fig. 15 we show the modified F(x) after such a subtraction of "elastic" ρ^{0} events as well as the contribution to F(x) from the eliminated events. We find that the π^{-} mesons from elastic ρ^{0} events do not influence F(x) for $x < 0$. (The small contribution at 2.8 and 4.7 GeV for $x < 0$ is mainly due to inclusion of background under the ρ^{0} resonance which decreases rapidly with increasing energy.) As seen in Fig. 15d, e the comparison of the 4.7 and 9.3 GeV data shows that exclusion of elastic ρ^{0} events does not alter our conclusions about scaling.

To further explore the composition of the structure function, we give in Fig. 16 F(x) for the separate charged multiplicities at 9.3 GeV. The curves show the contributions from the events having no missing neutrals, a single π^{0} missing, a single neutron missing and from multineutral events.[18] We see that almost all the contributions to F(x) at large x come from 3 and 4 body production in the 3-prong events. By eliminating these events we obtain the dotted curve in Fig. 16 (top). This distribution (for 5 or more bodies with at least 2 neutrals) is somewhat similar in shape (though not in magnitude) to the 5-prong distribution which suggests that the neutral pion distributions may be like those of the charged pions.

FACTORIZATION OF THE STRUCTURE FUNCTION

In the reaction $pp \rightarrow \pi^- + $ (anything) above 12 GeV/c, N. F. Bali et al.[19] found that the x and $p_\perp^2$ dependence of the structure function was uncoupled, i.e., they could fit the data with a factorized form for the structure function,

$$f_3(x, p_\perp^2) = G(x)\ H(p_\perp^2) \quad .$$

In contrast Ko and Lander[20] found in the reaction $K^+p \rightarrow \pi^- + $ (anything) at 11.8 GeV/c that $f_3(x, p_\perp^2)$ did not factorize in this way. To test whether the structure function in $\gamma p \rightarrow \pi^- + $ (anything) may be factorized we give in Fig. 17 plots of

$$F\left(x, \langle p_\perp^2 \rangle\right) = \frac{1}{\pi} \int_a^b \frac{E^*}{p^*_{max}} \frac{d^2\sigma}{dx dp_\perp^2} dp_\perp^2 \quad ,$$

where a and b are the limits of the various $p_\perp^2$ intervals shown. The distributions in $F(x, \langle p_\perp^2 \rangle)$ do not have the same shape for all intervals of $p_\perp^2$, i.e., the structure function does not factorize. This is also seen in Fig. 18 where we display

$$f_3(x, p_\perp^2) = \frac{1}{\pi} \frac{E^*}{p^*_{max}} \frac{\Delta^2\sigma}{\Delta x \Delta p_\perp^2}$$

for the different x-intervals indicated.

The qualitative changes in the $p_\perp^2$ dependence of the structure functions are more clearly seen in Fig. 18b where three x-regions are shown in an expanded scale. The exponential decrease of $f_3(x, p_\perp^2)$ with $p_\perp^2$ is faster near x=0 than for other x-intervals. Yen and Berger[21] and Berger and Krzywicki[22] have suggested that the increase in the concentration of pions at small x and $p_\perp^2$ is due to generation of pions which are decay products of resonances (e.g. $\Delta(1236)$, $N^*(1680)$) with small Q-values.

From Fig. 18b we also see $f_3(x, p_\perp^2)$ flattens for the x-interval $0.3 < x < 0.5$ at small $p_\perp^2$ which is due to elastic ρ^0 events and their peripheral production mechanism and decay ($\sin^2\theta$ in the helicity system) into $\pi^+\pi^-$.[7]

We now turn to a comparison of the structure function for different charge multiplicities. J. Friedman[23] and Berger and Krzywicki[22] have pointed out that there is a phase space effect: as the multiplicity increases the dimensionality of phase space increases favoring pions at smaller c.m.s. momenta. This causes a more rapid falloff both in x (as seen in Fig. 16) and $p_\perp^2$. Therefore, we would expect the structure function for higher charged multiplicities (more prongs) to show a steeper falloff in $p_\perp^2$ at any x. The same is expected for higher neutral multiplicities. Since we can not separate events with different numbers of neutral particles, this effect will cause a steepening of the $p_\perp^2$ distribution of the π^- mesons at small $|x|$ for a given charged multiplicity.

In Fig. 19 we show that the transverse momentum dependence changes with x at a given multiplicity. The straight lines are exponential fits to the data for $p_\perp^2 < 0.3\ (\mathrm{GeV}/c)^2$. The exponential slope A from these fits is given in Table I. There is a steeper falloff in $p_\perp^2$ (as seen by larger values of A) as the multiplicity increases. Also, at a fixed multiplicity the falloff is steeper in the interval $-0.1 < x < 0.1$ than for other x regions. Thus our data seem to support the kinematic argument.

AVERAGE π^- MULTIPLICITY AND SCALING

Scaling predicts that at sufficiently high energy the π^- multiplicity $\langle n^-\rangle$ will obey the relation

$$\langle n^- \rangle = c^- \ln s + d^- , \qquad (7)$$

where c^- and d^- are energy independent.[19,24] It is interesting to investigate how well this form describes the data at our finite energies. In Fig. 20 we show the average charged-prong and π^- multiplicities for our four photon energies. For $\langle n^- \rangle$ we find the form of Eq. (7) fits well with $c^- = 0.44 \pm 0.04$ and $d^- = 0.07 \pm 0.08$ (for s in GeV^2). However, we also find the dependence of $\langle n^- \rangle$ on s is compatible with a power law behavior.

Following Bali et al.[19] we can approximately calculate c^- from the structure function. The average π^- multiplicity is

$$\langle n^- \rangle = \frac{\sum n^- \sigma_{n^-}}{\sigma_{TOT}} ,$$

where σ_{n^-} is the topological cross section for production of n^- negative pions. Then, because the inclusive cross section, $d^2\sigma$, counts the production of n^- negative pions n^- times, $\sum n^- \sigma_{n^-} = \iint d^2\sigma$ and

$$\langle n^- \rangle = \frac{\pi}{\sigma_{TOT}} \iint dx\, dp_\perp^2 \frac{f_3(x, p_\perp^2)}{\left(x^2 + \frac{p_\perp^2 + \mu^2}{p_{max}^{*2}}\right)^{1/2}} ,$$

where μ is the pion mass. Expanding f_3 about $x = 0$ we find[24]

$$\langle n^- \rangle = \frac{\pi}{\sigma_{TOT}} \left[\int_0^\infty dp_\perp^2\, f_3(0, p_\perp^2)\right] \ln s + \text{constant} + 0\left(\frac{1}{s} \ln s\right) , \quad (8)$$

where we have used the approximation $p_{max}^* \simeq \sqrt{s}/2$. For our data the quantity in brackets is just F(0) which is plotted in Fig. 12 and is 14.7 ± 1.0, (16.0 ± 0.7), $\langle 17.1 \pm 0.7 \rangle$ μb at 2.8, (4.7), $\langle 9.3 \rangle$ GeV (a small correction $< 1.3\%$ has been applied to correct F(0) for the strange particle events). Using for σ_{TOT} our values of 133 ± 3, (127 ± 3), $\langle 122 \pm 4 \rangle$ μb, we find for the coefficient of $\ln s$ values of 0.35 ± 0.03, (0.40 ± 0.02), $\langle 0.44 \pm 0.02 \rangle$ at 2.8, (4.7), $\langle 9.3 \rangle$ GeV which are similar to the slope $c^- = [0.44 \pm 0.04]$ found from the fit to the measured π^- multiplicity. The increase of c^- with increasing energy is caused by the decrease of the total cross section ($\sim 4\%$ between energies) and the increase of the integrated structure function at x=0 ($\sim 7\%$ between energies). It is interesting that the approximations used in deriving Eq. (8) seem to be quite good at our moderate energies.

We remark that any reasonably smooth scaling distribution in x and $p_\perp^2$ results at very high energy in a y-distribution having limiting fragmentation and a flat region in $d\sigma/dy$ (in fact, if $f_3(x, p_\perp^2)$ exhibits scaling for all incident particles, properties (i), (ii), and (iii) previously mentioned in the section on the rapidity variable will follow). In particular, a flat plateau in $d\sigma/dy$ (presumably indicating pionization) is predicted (a fixed interval in x of width ϵ about $x=0$ transforms into a region in y of width $\ln(s\epsilon^2)$ and height $\pi F(x=0)$). Alternatively, a flat region in $d\sigma/dy$ would lead to a $\ln s$ increase of the average multiplicity $\langle n^- \rangle$ and scaling in x. However, at our relatively low photon energies no clear flat region in $d\sigma/dy$ is seen (Fig. 10). Nevertheless, the integral of $\frac{1}{\sigma_{TOT}} \frac{d\sigma}{dy}$ is increasing as $\ln s$ thus giving $\langle n^- \rangle \alpha \ln s$. This behavior is unrelated to an extended flat region and thus from our data we are unable to establish pionization as the mechanism responsible for the increase of $\langle n^- \rangle$.

REGGE TRAJECTORIES AND THE STRUCTURE FUNCTION

Feynman has suggested[2] that if scaling occurs, then, at the extremes of x one should have

$$f(x,t) = (1 - |x|)^{1-2\alpha(t)} \quad , \tag{9}$$

where $\alpha(t)$ is the highest Regge trajectory that could carry off the quantum numbers and momentum transfer at the $\gamma \to \pi$ (at $x=1$) and $p \to \pi$ ($x=-1$) vertices.

Such behavior can also be predicted by the multiperipheral model. Caneschi and Pignotti[25] using a multi-Regge model for the part of the cross section due to the diagrams of Fig. 21 have obtained the following expression (in the limit of large s, large missing-mass squared, s', and large ratio s/s'):

$$\frac{d^3\sigma}{d^3\vec{p}} = \frac{1}{E}\left(\frac{s}{s'}\right)^{2\alpha(t)-1} |G(t)|^2 \, \sigma_R^{TOT}(s',t) \quad . \tag{10}$$

Here $\alpha(t)$ is the Regge trajectory exchanged, which is coupled to the proton (photon) with a residue function G(t). $\sigma_R^{TOT}(s',t)$ is to be interpreted as a Reggeon-photon (proton) total cross section. Now, in terms of the c.m.s. energy E* of the outgoing π^-

$$\frac{s'}{s} = \frac{\mu^2}{s} + 1 - \frac{2E^*}{\sqrt{s}} \sim 1 - |x|$$

for s large and $p_\parallel^2 >> p_\perp^2 + \mu^2$. If we assume $\sigma_R^{TOT}(s',t)$ to be asymptotically constant in s', we obtain Eq. (9) after equating

$$f(x,t) = E\,\frac{d^3\sigma}{d^3\vec{p}} \quad .$$

We have determined $\alpha(t)$ in Eq. (10) by fitting the experimental distribution for our 9.3 GeV data to $\left(\frac{s'}{s}\right)^{1-2\alpha(t)}$ for finite t-intervals. We fitted over two ranges: $a < \frac{s'}{s} < 0.7$ for the target region and $b < \frac{s'}{s} < 0.5$ for the beam region. The limits $a \sim 0.25$ and $b \sim 0.1$ were adjusted for each t-interval to avoid effects due to the kinematic boundary in $\left(\frac{s'}{s}\right)$ and t. While $s = 18.3\ \mathrm{GeV}^2$ may be considered large, we recognize that the lower limits, $s' = 1.8$ GeV and $\left(\frac{s}{s'}\right) = 1.4$ are not large as was required in the derivation of Eq. (10).

In Fig. 22a we give resulting values of $\alpha(t)$ for the $p \to \pi$ vertex (target region and diagram of Fig. 21a). The values of $\alpha(t)$ are much lower than the known leading Regge trajectory (Δ in this case)[26] but similar to those obtained from other inclusive experiments,[27,28] e.g., $pp \to \pi^- +$ (anything). Discussion of this discrepancy can be found in Refs. 27 and 28.

In Fig. 22b we give $\alpha(t)$ for the $\gamma \to \pi$ vertex. (Elastic ρ^0 events have been included.) Here the $\alpha(t)$ is compatible with a Regge trajectory of slope 1 GeV^{-2} and $\alpha(0) = 0$; from VDM we would expect this trajectory to be associated with the pion.

POLARIZATION DEPENDENCE

Next we look for a correlation between the azimuthal angle ϕ of the π^- and the polarization vector ϵ of the photon: 93, (91), <77>% average polarization at 2.8, (4.7), <9.3> GeV . We define ϕ as

$$\phi = \tan^{-1}\left[\frac{\hat{k} \times \hat{\epsilon} \cdot \vec{p}_\perp}{\hat{\epsilon} \cdot \vec{p}_\perp}\right]$$

where $\hat{k}$ is a unit vector in the direction of the incident photon. In Fig. 23 we show for the 9.3 GeV data

$$\frac{d\sigma}{d\phi} = \frac{1}{\pi}\int_{x_1}^{x_2} dx \int_0^\infty dp_\perp^2 \; \frac{E^*}{p^*_{max}} \; \frac{d^3\sigma}{dx\,dp_\perp^2\,d\phi}$$

for various x-intervals. Here, the elastic ρ^0 production events and the residual events are shown separately. A fit to the data to the form $\frac{d\sigma}{d\phi} = (A + B\cos^2\phi)$ results in values for A and B given in Table II for the three energies (no correction has been applied to account for the unpolarized component in the beam). We find no statistically significant correlation between the π^- and the polarization vector for $x < 0.3$. However, some correlation is present for $x > 0.3$. On the other hand, even for $x > 0$ elastic ρ^{o} events show a strong correlation. The lack of correlation of the π^{-} with the polarization vector for $x < 0.0$ is consistent with factorization (in the Regge sense) of the residues of the photon and target vertices.[29]

LORENTZ FRAME FOR A SYMMETRIC LONGITUDINAL MOMENTUM DISTRIBUTION

The F(x) distributions showed an asymmetry about $x=0$ (see Fig. 12, 15) which has also been found in inclusive $\pi^{-}p$ studies. In the case of $\pi^{-}p$ reactions, Elbert et al.[30] studied the composite $p_{\parallel}$ distribution in the c.m.s. of backward π^{-} and forward π^{+} and found that by Lorentz transforming to a frame where the ratio R of the incident proton momentum to the incident π^{-} momentum is 1.5 (the "Q-system" in their notation), the longitudinal momentum distribution of the π becomes symmetric. This result has been interpreted in the framework of the quark model. If there are 2 quarks in the π and 3 quarks in the proton, in this "quark" frame all five quarks have the same average value of $|p|$. Thus, in this interpretation the symmetric distribution for $R = 1.5$ results from symmetry in the quark-quark center-of-mass system for the quark-quark collision that takes place.

In Fig. 24 we show the $p_{\parallel}$ distribution for the 9.3 GeV photon data in the frames where $R = 1.0$, 1.5, and 2.3. $R = 2.3$ yields a symmetric distribution. Here we have excluded elastic ρ^{o} production as before. Table III gives the values of R needed to obtain symmetry at our three energies. We also determined the symmetric frame with elastic ρ^{o} events included and Table III shows even larger values of R (~ 3) in this case. We conclude that the Q-system does not give symmetry for photoproduced π^{-}. In the spirit of the Q-system argument, a value of R=3 would suggest that the photon interacts as a single quark-like object with one of the three quarks of the proton.

CONCLUSIONS

1. We find a decrease of $E\frac{d\sigma}{dp_{\parallel}}$ in the target region ($p_{\parallel}$ < 300 MeV) with increasing photon energy. Thus limiting target fragmentation in the strict sense of Ref. 1 is not observed. The energy dependence of $E\frac{d\sigma}{dp_{\parallel}}$ is compatible with approaching a limiting distribution as $A+Bs^{-1/2}$ as predicted by Chan et al [12] (Fig. 4,6).

2. We observe a significant decrease in $d\sigma/dy$ with increasing photon energy both in the target and beam fragmentation regions. For the central region of the "rapidity" distribution no extended flat region is observed (Fig. 10).

3. The qualitative features of the structure function in terms of Feynman's x-variable are similar for all x at the three energies. There are, however, small but statistically significant differences between the three energies (Fig. 12,13).

4. We find that the structure function $f_3(x, p_{\perp}^2)$ does not factorize into independent functions of x and $p_{\perp}^2$ (Fig. 17,18).

5. Even at our moderate photon energies (1.4 GeV to 9.3 GeV) the increase in π^- multiplicity is consistent with a logarithmic growth in s (Fig. 20).

6. When interpreted in a Regge framework, the t dependence of the structure function leads to a trajectory associated with the $\gamma \to \pi^-$ vertex (forward π^- production) with $\alpha(0) \approx 0.0$ and a slope ≈ 1 GeV^{-2}; for the trajectory associated with the $p \to \pi^-$ vertex (backward π^- production) one obtains a similar slope but an $\alpha(0)$ which is lower than that of the expected leading trajectory (the Δ) (Fig. 22).

7. There is no azimuthal correlation of the outgoing π^- and the polarization vector of the incident photon for $x < 0$. For $x > 0$ we find a significant correlation approximately half of which comes from elastic ρ^0 production (Fig. 23 and Table II).

8. The Q-system of Elbert et al.,[30] does not result in a symmetric distribution in $p_{\parallel}$ for the π^-. We find at 9.3 GeV that symmetry is reached for the ratio of colliding momenta R = 2.3 with elastic ρ^0 removed and R = 2.75 with elastic ρ^0 included (Fig. 24 and Table III).

9. When scaled by the total cross section our inclusive π^- cross sections in the target region are similar to those found in π^-p reactions. They are larger by a factor of ≈ 2 than those obtained from π^+p, K^+p and pp reactions (Fig. 7, 14).

ACKNOWLEDGEMENTS

We acknowledge the stimulating discussions we have had with Professors J. D. Bjorken, H. Abarbanel, and Dr. C. Risk. We wish to thank the SLAC operations crew of the accelerator and R. Watt and the 82" bubble chamber operation group. The diligent work of the scanners at SLAC and Berkeley is gratefully acknowledged. We gratefully acknowledge the contribution of W. R. Graves, Dr. Jim Murray, and Dr. G. Smadja.

REFERENCES

1. J. Benecke, T. T. Chou, C. N. Yang, and E. Yen, Phys. Rev. 188, 2159 (1969).

2. R. P. Feynman, Phys. Rev. Letters 23, 1415 (1969); R. P. Feynman, The Behavior of Hadron Collisions at Extreme Energies, California Institute of Technology report (1969); see also High Energy Collisions (Gordon and Breach, New York, 1969), p. 237.

3. K. G. Wilson, Acta Phys. Austr. 17, 37 (1963); Kenneth G. Wilson, Cornell Preprint CLNS-131 (1970).

4. Carleton E. DeTar, Phys. Rev. D3, 128 (1971). The literature concerning multiperipheral models and their predictions for the inclusive reactions can be traced from this publication.

5. As suggested by Feynman (private communication) we use $x = p^*_\parallel / p^*_{max}$ with $-1 \leq x \leq 1$ at our finite energies instead of the asymptotic form $x = 2p^*_\parallel/\sqrt{s}$ given in Ref. 2.

6. J. C. Vander Velde, Phys. Letters 32B, 501 (1970).

7. J. Ballam, G. B. Chadwick, R. Gearhart, Z.G.T. Guiragossián, P. R. Klein, A. Levy, M. Menke, J. J. Murray, P. Seyboth, G. Wolf, C. K. Sinclair, H. H. Bingham, W. B. Fretter, K. C. Moffeit, W. J. Podolsky, M. S. Rabin, A. H. Rosenfeld, and R. Windmolders, Phys. Rev. Letters 23, 498 (1969); 23, 817(E) (1969). For other experimental details and results of this experiment see H. H. Bingham et al., Phys. Rev. Letters 24, 955 (1970); J. Ballam et al., Phys. Rev. Letters 24, 960 (1970); 1467(E) (1970); J. Ballam et al., SLAC-PUB-941 (1971).

8. M. Rabin, H. H. Bingham, W. B. Fretter, W. J. Podolsky, A. H. Rosenfeld, G. Smadja, G. Wolf, J. Ballam, G. B. Chadwick, M. Della Negra,

R. Gearhart, M. Menke, K. C. Moffeit, J. J. Murray, P. Seyboth, C. K. Sinclair, I. O. Skillicorn, H. Spitzer, and R. H. Milburn, "Total and Partial Photoproduction Cross Sections at 9.5 GeV," Bull. Am. Phys. Soc., Series 11, Vol. 15, No. 12, 1634 (1970).

9. For example, see D. B. Smith et al., Phys. Rev. Letters 23, 1064 (1969).

10. See also W. P. Swanson, M. Davier, I. Derado, D. C. Fries, F. F. Liu, R. F. Mozley, A. Odian, J. Park, F. Villa, and D. Yount, Phys. Rev. Letters 27, 1472 (1971). These authors used the SLAC streamer chamber and a bremsstrahlung photon beam with photon energies from 5 to 18 GeV and report a similar energy dependence for $d\sigma/dp_{\parallel}$ in the region $p_{\parallel} < 500$ MeV.

11. A. H. Mueller, Phys. Rev. D2, 2963 (1970).

12. Chan Hong-Mo, C. Hsue, C. Quigg, and Jiunn-Ming Wang, Phys. Rev. Letters 26, 672 (1971).

13. M.-S. Chen, R. R. Kinsey, T. W. Morris, R. S. Panvini, L.-L. Wang, T. F. Wong, S. L. Stone, T. Ferbel, P. Slattery, B. Werner, J. W. Elbert, and A. R. Erwin, Phys. Rev. Letters 26, 1585 (1971).

14. For the asymptotic values of the total cross sections, M.-S. Chen et al., (Ref. 13) use 23.4, 17.4, 39.8, and 24.9 mb for π^+p, K^+p, pp, and π^-p incident channels, respectively. For γp we use $\sigma_{TOT}(\infty) = 99\ \mu b$ which results from a fit to the form $\sigma_{TOT}(s) = a + B\, s^{-1/2}$ by Hesse et al. (Ref. 15). Corrections were also applied to the γp data to account for the π^- production in the strange particle topologies.

15. W. P. Hesse, D. O. Caldwell, V. B. Elings, R. J. Morrison, F. V. Murphy, B. W. Worster, and D. E. Yount, Phys. Rev. Letters 25, 613 (1970).

16. We know of no experiment that has shown a flat distribution in y. The Echo Lake experiment shows distributions in $\log_{10} \tan \theta_{lab}$ which for $p_{\parallel} \gg p_{\perp} \gg M_{\pi}$ is related to y ($y \simeq \ln(2/\tan \theta_{lab})$); they obtain distributions which show no clear flat central region at energies 146 and 211 GeV. L. W. Jones et al., Phys. Rev. Letters 25, 1679 (1970); D. E. Lyon, Jr. et al., Phys. Rev. Letters 26, 728 (1971).

17. W. D. Shephard, J. T. Powers, N. N. Biswas, N. M. Cason, V. P. Kenny, R. R. Riley, D. W. Thomas, J. W. Elbert, and A. R. Erwin, Phys. Rev. Letters 27, 1164 (1971).

18. The curves for final states with a single π^o or neutron were obtained from all events with an appropriate 0-C "fit" with neutral missing mass squared MM^2 in the regions $-0.08<(MM)^2<0.12$ GeV^2 and $0.65<(MM)^2<1.1$ GeV^2, respectively. No further cuts or corrections were applied.

19. N. F. Bali, L. S. Brown, R. D. Peccei, and A. Pignotti, Phys. Rev. Letters 25, 557 (1970). Because the experimental pp data used was limited to x-values $\gtrsim 0.05$, this work did not test the factorization hypothesis at $x \simeq 0$ where the K^+p (see Ref. 20) and γp (this experiment) data have the greatest change of the structure function dependence on transverse momentum.

20. W. Ko and R. L. Lander, Phys. Rev. Letters 26, 1064 (1971).

21. Edward Yen and Edmond L. Berger, Phys. Rev. Letters 24, 695 (1970).

22. Edmond L. Berger and A. Krzywicki, Laboratoire de Physique Théorique et Particules Elémentaires, Orsay, Preprint-71/36.

23. J. Friedman (private communication).

24. Here we briefly rederive the results of Bali et al. (Ref. 19) giving Eq. (8). At high energies, the contribution to the integral

$$\langle n^- \rangle = \frac{\pi}{\sigma_{TOT}} \int_0^\infty dp_\perp^2 \int_{-1}^1 dx \, \frac{f_3(x, p_\perp^2)}{\left(x^2 + \frac{p_\perp^2 + \mu^2}{p_{max}^{*2}} \right)^{1/2}}$$

comes mainly from the vicinity of x=0. For convenience let

$$a \equiv \frac{(p_\perp^2 + \mu^2)^{1/2}}{p^*_{max}} , \qquad f = f_3(0, p_\perp^2), \quad f' = \left. \frac{\partial f_3}{\partial x} \right|_{x=0} , \text{ etc.}$$

After expanding $f_3(x, p_\perp^2)$ about x=0

$$f_3(x, p_\perp^2) = f + x f' + \frac{x^2}{2} f'' + \ldots$$

we find

$$\int_{-1}^1 dx \frac{f_3(x, p_\perp^2)}{(x^2+a^2)^{1/2}} = f \int_{-1}^1 \frac{dx}{(x^2+a^2)^{1/2}} + f' \int_{-1}^1 \frac{x\,dx}{(x^2+a^2)^{1/2}} + \frac{f''}{2} \int_{-1}^1 \frac{x^2\,dx}{(x^2+a^2)^{1/2}} + \ldots$$

$$= 2 \left[f - \frac{a^2}{4} f'' \right] \ln \left[\frac{1 + \sqrt{1+a^2}}{a} \right] + \frac{1}{2} f'' \sqrt{1+a^2} + \ldots$$

$$\xrightarrow[s \to \infty]{} \left[f - \frac{(p_\perp^2+\mu^2)}{s} f'' \right] \ln \left[\frac{s}{p_\perp^2+\mu^2} \right] + \frac{1}{2} f'' \left(1 + 2 \, \frac{(p_\perp^2+\mu^2)}{s} \right) + \ldots .$$

where we have used $p^*_{max} \sim \sqrt{s}/2$. Integrating over $dp_\perp^2$, we find

$$\langle n^- \rangle = \left[\frac{\pi}{\sigma_{TOT}} \int_0^\infty dp_\perp^2 \; f_3(0, p_\perp^2) \right] \ln s + \text{const} + 0 \, \frac{\ln s}{s}$$

provided that:

(i) $f_3(x, p_\perp^2)$ scales and reaches a nonzero limit at x=0,

(ii) the integral over $dp_\perp^2$ converges, i.e., the distribution in $p_\perp^2$ is limited e.g., as $\exp(-A\, p_\perp^2)$,

(iii) the total cross section is asymptotically finite.

25. L. Caneschi and A. Pignotti, Phys. Rev. Letters 22, 1219 (1969).

26. V. D. Barger and D. B. Cline, Phenomenological Theories of High Energy Scattering (W. A. Benjamin, Inc., New York, 1969), p. 126.

27. R. D. Peccei and A. Pignotti, Phys. Rev. Letters 26, 1076 (1971).

28. Clifford Risk, UCRL-20841, Lawrence Berkeley Laboratory (1971).

29. H. Abarbanel and D. Gross, Phys. Rev. Letters 26, 732 (1971).

30. J. Elbert, A. R. Erwin, and W. D. Walker, Phys. Rev. D3, 2042 (1971).

TABLE I

Values of the exponential slope A $(\mathrm{GeV}/c)^{-2}$ fitting the structure function $F(\langle x\rangle, p_\perp^2)$ of Fig. 19 for $p_\perp^2 < 0.3\ (\mathrm{GeV}/c)^2$ to $F(\langle x\rangle, p_\perp^2) = F(\langle x\rangle, 0) \exp(-A p_\perp^2)$.

x	3-prongs*	5-prongs*	7-prongs*	9-prongs*
(-1.0)-(-0.1)	5.3 ± 0.5	6.4 ± 0.4	7.2 ± 0.9	12.5 ± 4.3
(-0.1)-(0.1)	7.3 ± 0.3	7.9 ± 0.3	9.2 ± 0.4	11.9 ± 1.5
(0.1)-(0.4)	6.0 ± 0.3	6.1 ± 0.3	6.8 ± 0.6	7.8 ± 2.4
(0.4)-(1.0)	6.8 ± 0.3	6.2 ± 0.6	7.2 ± 2.9	—

*An N-prong event has N charged particles without detected strange-particle decay.

TABLE II

Value of A and B fitting $d\sigma/d\phi$ to the form $d\sigma/d\phi = (A + B \cos^2 \phi)$

E_γ (GeV)	x	Elastic ρ^o excluded[a]		Elastic ρ^o only[a]	
		A(nb/deg)	B(nb/deg)	A(nb/deg)	B(nb/deg)
2.8	(-1.0) - (-0.3)	2.80 ± 0.22	0.24 ± 0.37	0.24 ± 0.08	0.07 ± 0.13
	(-0.3) - (0.0)	7.36 ± 0.29	0.17 ± 0.47	0.29 ± 0.06	0.28 ± 0.11
	(0.0) - (0.3)	9.65 ± 0.33	0.73 ± 0.55	0.89 ± 0.12	2.65 ± 0.25
	(0.3) - (1.0)	7.60 ± 0.39	2.24 ± 0.66	7.06 ± 0.41	5.42 ± 0.73
4.7	(-1.0) - (0.3)	2.16 ± 0.14	-0.18 ± 0.22	0.04 ± 0.03	0.05 ± 0.05
	(-0.3) - (0.0)	7.82 ± 0.21	0.22 ± 0.36	0.04 ± 0.02	0.00 ± 0.02
	(0.0) - (0.3)	11.51 ± 0.25	-0.05 ± 0.41	0.43 ± 0.06	1.40 ± 0.13
	(0.3) - (1.0)	8.38 ± 0.30	2.61 ± 0.52	4.30 ± 0.25	5.21 ± 0.46
9.3[b]	(-1.0) - (-0.3)	1.55 ± 0.12	0.08 ± 0.20	—	—
	(-0.3) - (0.0)	7.95 ± 0.19	-0.03 ± 0.30	—	—
	(0.0) - (0.3)	12.87 ± 0.25	0.45 ± 0.42	0.21 ± 0.04	0.77 ± 0.08
	(0.3) - (1.0)	9.48 ± 0.33	2.29 ± 0.56	3.41 ± 0.22	3.53 ± 0.41

[a] Elastic ρ^o event: $\gamma p \rightarrow \pi^-\pi^+p$ with $M_{\pi^+\pi^-} < 1.0$ GeV.

[b] Data plotted in Fig. 23.

TABLE III

Value of $R = \frac{p_{proton}}{p_{photon}}$ for the frame in which the π^- longitudinal momentum distribution is symmetric.

E_γ (GeV)	R	
	elastic ρ^o excluded*	elastic ρ^o included*
2.8	1.75 ± 0.05	2.95 ± 0.1
4.7	1.85 ± 0.05	2.75 ± 0.1
9.3	2.3 ± 0.05	2.75 ± 0.1

*elastic ρ^o event: $\gamma p \rightarrow \pi^+\pi^- p$ with $M_{\pi^+\pi^-} < 1.0$ GeV

TABLE IV

The structure function $\mathscr{F}(p_{\parallel})$ in the laboratory. The central value of $p_{\parallel}$ and the bin width are labelled $p_{\parallel}$ and $\Delta p_{\parallel}$, respectively. Data plotted in Fig. 4.

$p_{\parallel}$ (GeV/c)	$\Delta p_{\parallel}$ (GeV/c)	$\mathscr{F}(p_{\parallel})$ (μb) E_γ = 2.8 GeV		E_γ = 4.7 GeV		E_γ = 9.3 GeV	
-0.225	0.15	1.736 ±	0.203	1.165 ±	0.132	0.666 ±	0.104
-0.075	0.15	7.217	0.387	5.634	0.261	4.076	0.227
0.025	0.05	13.229	0.914	11.839	0.653	9.100	0.598
0.075	0.05	20.223	1.158	16.567	0.774	12.998	0.733
0.125	0.05	26.759	1.391	19.688	0.890	16.508	0.844
0.175	0.05	27.749	1.453	25.034	1.055	21.819	1.028
0.225	0.05	30.632	1.630	26.860	1.131	23.492	1.136
0.275	0.05	35.513	1.855	34.188	1.361	30.846	1.367
0.325	0.05	40.103	2.063	35.996	1.445	31.732	1.440
0.375	0.05	41.942	2.167	37.591	1.544	34.655	1.563
0.425	0.05	45.778	2.379	38.823	1.556	37.600	1.713
0.475	0.05	46.073	2.464	44.494	1.835	41.177	1.863
0.525	0.05	46.508	2.580	43.198	1.876	42.665	1.985
0.575	0.05	40.003	2.459	46.462	2.022	44.287	2.079
0.625	0.05	47.326	2.759	45.964	2.076	43.906	2.137
0.675	0.05	44.803	2.780	45.351	2.126	44.954	2.235
0.725	0.05	40.823	2.720	44.483	2.167	44.920	2.311
0.775	0.05	46.811	3.008	46.750	2.278	51.350	2.542
0.825	0.05	47.409	3.101	49.418	2.411	45.318	2.448
0.875	0.05	42.256	3.004	44.610	2.348	48.754	2.594
0.925	0.05	37.472	2.889	43.833	2.383	53.250	2.784
0.975	0.05	44.221	3.214	46.334	2.507	50.991	2.784
1.050	0.10	44.362	2.345	43.600	1.781	52.972	2.085
1.150	0.10	42.333	2.386	45.739	1.900	52.765	2.161
1.250	0.10	47.732	2.626	47.759	2.017	51.096	2.212
1.350	0.10	43.663	2.602	43.421	1.988	53.178	2.335
1.450	0.10	41.110	2.607	43.082	2.046	53.309	2.415
1.550	0.10	37.767	2.577	44.306	2.149	48.655	2.378
1.650	0.10	39.315	2.701	43.014	2.179	49.791	2.484
1.750	0.10	35.630	2.641	36.540	2.063	49.775	2.551
1.850	0.10	28.813	2.444	36.920	2.129	50.479	2.642
1.950	0.10	25.508	2.358	43.283	2.366	45.405	2.561
2.100	0.20	26.584	1.757	38.895	1.646	48.413	1.944
2.300	0.20	25.638	1.809	36.418	1.665	46.638	1.989
2.500	0.20	23.195	1.784	35.719	1.719	49.251	2.125
2.700	0.20	6.969	1.006	35.350	1.777	47.905	2.182
2.900	0.20	0.461	0.266	31.656	1.740	46.698	2.225
3.100	0.20	0.0	0.0	28.623	1.711	47.082	2.310
3.300	0.20	0.0	0.0	28.680	1.772	43.251	2.281
3.500	0.20	0.0	0.0	24.817	1.697	43.025	2.342
3.700	0.20	0.0	0.0	15.238	1.369	38.067	2.256
3.900	0.20	0.0	0.0	15.119	1.398	41.423	2.421
4.250	0.50	0.0	0.0	10.149	0.757	37.506	1.521
4.750	0.50	0.0	0.0	1.356	0.289	33.545	1.519
5.250	0.50	0.0	0.0	0.0	0.0	32.723	1.575
5.750	0.50	0.0	0.0	0.0	0.0	30.022	1.581
6.250	0.50	0.0	0.0	0.0	0.0	26.532	1.545
6.750	0.50	0.0	0.0	0.0	0.0	23.726	1.519
7.250	0.50	0.0	0.0	0.0	0.0	17.569	1.351
7.750	0.50	0.0	0.0	0.0	0.0	13.797	1.239
8.250	0.50	0.0	0.0	0.0	0.0	10.636	1.121
8.750	0.50	0.0	0.0	0.0	0.0	6.513	0.903
9.250	0.50	0.0	0.0	0.0	0.0	3.432	0.673
9.750	0.50	0.0	0.0	0.0	0.0	0.554	0.277

1986B34

TABLE V

Differential π^- cross section $d\sigma/dy$. The central value of the "rapidity" y and the bin width are labelled y and Δy, respectively. Data plotted in Fig. 10.

y	Δy	$d\sigma/dy$ (μb)					
		E_γ = 2.8 GeV		E_γ = 4.7 GeV		E_γ = 9.3 GeV	
-0.900	0.20	2.592 ±	0.378	1.668 ±	0.231	0.865 ±	0.176
-0.700	0.20	1.873	0.321	1.157	0.192	1.073	0.196
-0.500	0.20	3.929	0.466	3.113	0.316	2.435	0.297
-0.300	0.20	7.123	0.630	5.381	0.415	3.751	0.367
-0.100	0.20	10.232	0.754	8.113	0.510	6.316	0.477
0.100	0.20	13.988	0.881	11.847	0.617	9.479	0.584
0.300	0.20	21.816	1.100	18.413	0.768	13.455	0.698
0.500	0.20	30.458	1.300	23.805	0.873	20.991	0.872
0.700	0.20	36.459	1.424	31.083	0.999	26.256	0.976
0.900	0.20	41.987	1.530	39.988	1.133	32.761	1.091
1.050	0.10	49.106	2.333	43.246	1.665	42.120	1.751
1.150	0.10	48.634	2.322	49.333	1.781	45.870	1.831
1.250	0.10	44.809	2.230	52.062	1.829	44.675	1.803
1.350	0.10	46.407	2.272	48.577	1.768	49.591	1.904
1.450	0.10	54.060	2.448	50.537	1.802	51.429	1.933
1.550	0.10	46.664	2.275	49.550	1.784	55.447	2.012
1.650	0.10	47.332	2.289	51.031	1.812	55.830	2.017
1.750	0.10	43.634	2.196	53.560	1.856	56.778	2.032
1.850	0.10	45.981	2.252	51.482	1.823	57.133	2.039
1.950	0.10	42.482	2.162	47.571	1.753	54.980	1.997
2.050	0.10	37.516	2.032	46.322	1.730	56.425	2.026
2.150	0.10	29.164	1.791	42.807	1.661	57.332	2.042
2.250	0.10	31.090	1.848	40.754	1.624	52.622	1.954
2.350	0.10	25.951	1.689	36.542	1.539	53.686	1.977
2.450	0.10	24.819	1.651	33.387	1.473	52.194	1.943
2.550	0.10	21.413	1.533	32.344	1.450	48.204	1.867
2.650	0.10	19.946	1.478	28.478	1.363	50.733	1.916
2.750	0.10	14.372	1.255	26.103	1.304	47.553	1.858
2.850	0.10	10.729	1.083	23.275	1.232	42.712	1.756
2.950	0.10	10.823	1.087	19.509	1.128	40.801	1.717
3.100	0.20	7.755	0.650	15.192	0.704	34.506	1.115
3.300	0.20	3.925	0.462	10.250	0.579	28.510	1.013
3.500	0.20	1.035	0.237	7.094	0.482	22.472	0.899
3.700	0.20	0.436	0.154	3.734	0.349	14.933	0.733
3.900	0.20	0.0	0.0	1.626	0.232	11.090	0.632
4.100	0.20	0.0	0.0	0.499	0.128	7.540	0.520
4.300	0.20	0.0	0.0	0.0	0.0	4.160	0.386
4.500	0.20	0.0	0.0	0.0	0.0	2.126	0.276
4.700	0.20	0.0	0.0	0.0	0.0	1.253	0.211
4.900	0.20	0.0	0.0	0.0	0.0	0.432	0.124

1986A35

TABLE VI

Structure function $F(x) = \frac{1}{\pi}\int_0^{\infty} \frac{E^*}{p^*_{max}} \frac{d^2\sigma}{dx\,dp_\perp^2}\,dp_\perp^2$. The central value of x and the bin width are labelled x and Δx, respectively. Data plotted in Fig. 12.

x	Δx	F(x) (μb) E_γ = 2.8 GeV		F(x) (μb) E_γ = 4.7 GeV		F(x) (μb) E_γ = 9.3 GeV	
-0.900	0.20	0.093 ±	0.038	0.085 ±	0.028	0.050 ±	0.022
-0.700	0.20	1.086	0.121	0.509	0.063	0.166	0.036
-0.550	0.10	1.673	0.201	1.105	0.120	0.858	0.109
-0.450	0.10	2.894	0.249	2.128	0.155	1.568	0.133
-0.350	0.10	4.753	0.301	3.413	0.180	2.917	0.169
-0.275	0.05	6.296	0.468	5.117	0.293	4.596	0.273
-0.225	0.05	7.176	0.471	6.648	0.320	5.761	0.291
-0.175	0.05	9.359	0.523	8.608	0.355	7.418	0.311
-0.125	0.05	10.032	0.524	10.466	0.370	9.950	0.334
-0.090	0.02	10.471	0.812	11.992	0.601	12.416	0.564
-0.070	0.02	13.586	0.957	13.400	0.638	13.742	0.576
-0.050	0.02	13.267	0.905	12.919	0.592	15.106	0.599
-0.030	0.02	12.495	0.856	14.242	0.648	15.183	0.579
-0.010	0.02	14.866	0.980	15.269	0.646	16.953	0.612
0.010	0.02	14.382	0.970	16.629	0.685	16.891	0.603
0.030	0.02	15.344	0.999	17.204	0.707	17.165	0.619
0.050	0.02	14.658	0.965	15.417	0.666	17.764	0.636
0.070	0.02	16.548	1.023	15.765	0.667	18.105	0.664
0.090	0.02	16.005	1.053	15.510	0.684	18.013	0.664
0.110	0.02	15.638	1.006	15.364	0.690	16.568	0.660
0.130	0.02	15.959	1.046	14.016	0.661	16.901	0.683
0.150	0.02	14.584	0.997	16.231	0.732	16.691	0.706
0.170	0.02	16.392	1.089	13.723	0.676	16.273	0.708
0.190	0.02	15.850	1.063	15.797	0.755	15.502	0.707
0.225	0.05	13.953	0.651	14.511	0.471	15.642	0.476
0.275	0.05	13.472	0.665	14.821	0.500	15.030	0.492
0.325	0.05	13.487	0.685	12.965	0.489	14.084	0.505
0.375	0.05	13.953	0.725	12.527	0.503	12.955	0.507
0.425	0.05	13.059	0.719	12.012	0.509	12.108	0.517
0.475	0.05	13.463	0.751	11.246	0.514	11.051	0.516
0.525	0.05	12.138	0.739	11.141	0.530	11.080	0.539
0.575	0.05	11.913	0.752	11.920	0.568	9.757	0.525
0.625	0.05	10.331	0.725	9.948	0.539	9.259	0.530
0.675	0.05	8.635	0.683	8.946	0.525	7.812	0.501
0.725	0.05	7.420	0.645	7.986	0.511	7.852	0.521
0.775	0.05	6.311	0.614	6.857	0.488	6.140	0.474
0.825	0.05	6.749	0.647	4.844	0.420	4.643	0.424
0.875	0.05	9.607	0.784	3.983	0.392	3.245	0.362
0.925	0.05	6.793	0.669	4.400	0.421	2.226	0.308
0.975	0.05	1.289	0.295	1.998	0.288	2.060	0.303

1986B32

TABLE VII

Structure function $F(x,<p_\perp^2>) = \frac{1}{\pi}\int_a^b \frac{E^*}{p^*_{max}} \frac{d^2\sigma}{dx dp_\perp^2} dp_\perp^2$ where a and b are the limits of the various $p_\perp^2$ intervals given. The column labelled x gives the central value and Δx the bin width. Data plotted in Fig. 17.

E_γ (GeV)	x	Δx	$F(x,<p_\perp^2>)$ (μb) $p_\perp^2 < 0.04$		$0.04 < p_\perp^2 < 0.16$		$0.16 < p_\perp^2 < 0.36$		$p_\perp^2 > 0.36$ (GeV/c)^2	
2.8	-0.900	0.20	0.047 ±	0.027	0.046 ±	0.026	0.0 ±	0.0	0.0 ±	0.0
	-0.700	0.20	0.282	0.058	0.445	0.076	0.294	0.065	0.064	0.032
	-0.500	0.20	0.559	0.072	0.839	0.092	0.527	0.031	0.349	0.072
	-0.350	0.10	1.014	0.120	1.810	0.175	1.140	0.155	0.787	0.146
	-0.250	0.10	1.805	0.140	2.359	0.184	1.704	0.133	0.866	0.151
	-0.150	0.10	2.451	0.145	3.835	0.221	2.686	0.222	0.672	0.133
	-0.075	0.05	3.599	0.229	4.783	0.232	2.816	0.316	1.203	0.242
	-0.025	0.05	3.871	0.229	5.613	0.359	3.105	0.333	0.790	0.199
	0.025	0.05	4.052	0.235	6.163	0.372	2.988	0.322	1.762	0.300
	0.075	0.05	4.498	0.258	6.146	0.378	3.730	0.362	1.432	0.273
	0.125	0.05	4.644	0.275	6.215	0.386	3.153	0.337	1.619	0.283
	0.175	0.05	3.790	0.264	7.719	0.449	2.904	0.328	1.322	0.261
	0.250	0.10	3.010	0.183	6.295	0.301	3.271	0.251	1.281	0.170
	0.350	0.10	2.776	0.197	6.180	0.320	3.930	0.289	0.832	0.152
	0.450	0.10	2.910	0.223	6.346	0.351	3.217	0.273	0.787	0.149
	0.550	0.10	2.978	0.245	5.538	0.351	2.771	0.266	0.738	0.151
	0.650	0.10	1.959	0.213	4.410	0.332	2.305	0.256	0.808	0.161
	0.750	0.10	1.759	0.216	3.120	0.297	1.784	0.236	0.201	0.082
	0.850	0.10	2.448	0.273	4.617	0.383	1.112	0.190	0.0	0.0
	0.950	0.10	2.773	0.302	1.268	0.205	0.0	0.0	0.0	0.0
4.7	-0.900	0.20	0.0 ±	0.0	0.035 ±	0.017	0.029 ±	0.017	0.020 ±	0.014
	-0.700	0.20	0.127	0.030	0.161	0.034	0.136	0.033	0.081	0.027
	-0.500	0.20	0.312	0.039	0.582	0.056	0.423	0.051	0.298	0.046
	-0.350	0.10	0.753	0.076	1.359	0.107	0.736	0.087	0.585	0.087
	-0.250	0.10	1.581	0.089	2.210	0.124	1.457	0.115	0.833	0.101
	-0.150	0.10	2.115	0.094	3.795	0.148	2.210	0.134	1.417	0.130
	-0.075	0.05	3.247	0.147	5.167	0.231	3.315	0.228	1.063	0.155
	-0.025	0.05	3.747	0.150	5.651	0.241	3.270	0.222	1.446	0.177
	0.025	0.05	4.604	0.165	6.656	0.257	3.649	0.236	1.823	0.207
	0.075	0.05	4.218	0.167	6.620	0.261	2.982	0.215	1.644	0.192
	0.125	0.05	3.663	0.169	6.822	0.277	3.056	0.222	1.377	0.179
	0.175	0.05	3.056	0.167	7.044	0.295	3.560	0.243	1.471	0.185
	0.250	0.10	2.824	0.129	6.415	0.214	3.778	0.186	1.649	0.143
	0.350	0.10	2.506	0.139	5.233	0.214	3.388	0.189	1.616	0.147
	0.450	0.10	2.442	0.154	5.012	0.230	2.984	0.185	1.191	0.133
	0.550	0.10	2.595	0.175	4.873	0.247	2.869	0.199	1.191	0.140
	0.650	0.10	2.249	0.175	3.657	0.230	2.453	0.196	1.087	0.138
	0.750	0.10	1.909	0.174	2.985	0.221	2.017	0.188	0.509	0.099
	0.850	0.10	0.976	0.131	2.151	0.199	1.101	0.147	0.184	0.061
	0.950	0.10	1.433	0.173	1.510	0.175	0.205	0.065	0.0	0.0
9.3	-0.900	0.20	0.009 ±	0.009	0.009 ±	0.009	0.0 ±	0.0	0.031 ±	0.018
	-0.700	0.20	0.014	0.009	0.077	0.024	0.031	0.015	0.043	0.019
	-0.500	0.20	0.216	0.035	0.379	0.046	0.262	0.039	0.354	0.050
	-0.350	0.10	0.456	0.061	0.907	0.089	0.815	0.089	0.738	0.093
	-0.250	0.10	1.139	0.083	1.609	0.104	1.453	0.108	0.975	0.101
	-0.150	0.10	1.920	0.088	3.277	0.129	2.019	0.116	1.466	0.118
	-0.075	0.05	3.228	0.135	5.464	0.214	3.031	0.192	1.835	0.183
	-0.025	0.05	4.176	0.139	6.453	0.221	3.279	0.196	1.892	0.184
	0.025	0.05	4.677	0.146	7.128	0.233	3.482	0.202	2.075	0.192
	0.075	0.05	4.403	0.159	7.644	0.252	3.724	0.212	2.041	0.191
	0.125	0.05	4.160	0.175	7.003	0.259	3.383	0.210	2.212	0.202
	0.175	0.05	3.454	0.178	6.501	0.268	3.698	0.229	2.361	0.211
	0.250	0.10	2.859	0.132	6.253	0.207	3.920	0.179	2.303	0.156
	0.350	0.10	2.490	0.143	5.517	0.221	3.676	0.190	1.835	0.149
	0.450	0.10	2.057	0.146	4.941	0.232	2.825	0.183	1.754	0.155
	0.550	0.10	1.995	0.159	4.045	0.230	2.881	0.199	1.495	0.152
	0.650	0.10	1.841	0.166	3.424	0.229	2.208	0.186	1.061	0.135
	0.750	0.10	1.718	0.171	2.692	0.217	1.610	0.169	0.976	0.136
	0.850	0.10	1.243	0.155	1.825	0.189	0.475	0.097	0.400	0.091
	0.950	0.10	0.979	0.146	0.718	0.125	0.355	0.088	0.090	0.045

1986B31

TABLE VIII

Structure function $f_3(x,p_\perp^2) = \dfrac{1}{\pi}\,\dfrac{E^*}{p^*_{max}}\,\dfrac{\Delta^2\sigma}{\Delta x \Delta p_\perp^2}$. The central value of $p_\perp^2$ and the bin width are labelled $p_\perp^2$ and $\Delta p_\perp^2$, respectively. Data plotted in Fig. 18.

E_γ (GeV)	$p_\perp^2$ $(GeV/c)^2$	$\Delta p_\perp^2$ $(GeV/c)^2$	$f_3(x,p_\perp^2)$ (μb) $-1.0<x<-0.3$	$-0.3<x<-0.1$	$-0.1<x<0.0$	$0.0<x<0.1$	$0.1<x<0.2$	$0.2<x<0.3$	$0.3<x<0.5$	$0.5<x<0.7$	$0.7<x<1.0$
2.8	0.005	0.01	12.98 ± 1.89	59.23 ± 5.11	111.30 ± 8.02	107.16 ± 7.91	110.76 ± 9.18	85.83 ± 9.46	75.69 ± 7.52	63.04 ± 8.17	45.17 ± 6.84
	0.015	0.01	9.87 1.47	57.63 5.21	89.42 7.77	114.71 8.84	120.79 10.08	67.27 8.57	81.65 8.03	67.85 8.57	72.83 8.50
	0.025	0.01	8.16 1.49	47.51 4.87	91.54 8.37	113.92 9.36	107.73 9.91	66.94 8.74	70.36 7.50	62.66 8.19	66.56 8.29
	0.035	0.01	9.91 1.65	48.48 5.03	81.32 8.27	91.77 8.60	82.47 8.91	81.00 9.84	56.66 6.76	53.35 7.65	48.15 7.04
	0.045	0.01	5.56 1.22	43.00 4.90	75.69 8.27	79.51 8.48	91.39 9.71	76.89 9.78	75.58 7.92	62.01 8.39	39.57 6.35
	0.055	0.01	5.74 1.24	33.86 4.40	59.22 7.59	74.40 8.49	79.84 9.30	65.62 9.20	66.49 7.42	46.86 7.34	36.23 6.06
	0.065	0.01	7.57 1.46	19.70 3.44	57.96 7.75	61.16 7.97	57.49 8.06	68.62 9.53	65.73 7.53	67.24 8.78	31.81 5.73
	0.075	0.01	4.00 1.09	32.83 4.57	45.40 7.01	74.61 8.99	65.27 8.69	53.41 8.56	59.42 7.24	41.74 6.57	23.98 4.91
	0.085	0.01	4.38 1.11	33.54 4.66	41.32 6.91	60.78 8.35	71.98 9.46	75.41 10.37	68.41 7.79	38.15 6.66	24.86 5.09
	0.095	0.01	5.55 1.27	20.73 3.73	45.66 7.41	52.04 7.85	60.65 8.85	55.50 9.01	43.21 6.19	62.22 8.57	25.19 5.05
	0.110	0.02	5.10 0.86	26.00 3.07	34.46 4.69	42.48 5.15	53.59 6.00	41.55 5.66	48.52 4.77	30.34 4.30	28.73 3.86
	0.130	0.02	5.70 0.96	23.65 2.90	43.26 5.41	31.71 4.63	47.74 5.88	30.51 4.96	35.56 4.15	27.15 4.06	15.43 2.82
	0.150	0.02	4.75 0.85	14.66 2.41	19.59 3.77	52.30 4.82	33.74 5.09	44.80 6.10	39.66 4.47	32.11 4.42	15.12 2.81
	0.170	0.02	3.41 0.73	15.41 2.50	24.76 4.40	35.68 5.21	20.74 4.07	34.59 5.47	25.40 3.60	19.92 3.58	10.95 2.39
	0.190	0.02	2.14 0.58	18.52 2.83	23.94 4.37	22.42 4.24	29.13 4.93	20.66 4.31	35.13 4.30	16.55 3.25	9.49 2.24
	0.225	0.05	2.05 0.38	11.11 1.44	19.57 2.59	18.06 2.51	15.80 2.36	19.79 2.77	22.41 2.22	16.65 2.10	6.37 1.16
	0.275	0.05	2.39 0.41	11.90 1.54	10.15 1.95	16.44 2.48	11.30 2.10	14.33 2.42	15.12 1.86	8.59 1.54	1.74 0.61
	0.325	0.05	1.28 0.31	6.87 1.22	9.25 1.93	8.18 1.83	10.54 2.11	7.86 1.85	8.04 1.40	9.44 1.65	2.61 0.75
	0.375	0.05	0.98 0.27	3.23 0.86	6.00 1.60	6.93 1.73	10.60 2.17	6.99 1.81	5.63 1.20	4.80 1.20	1.10 0.49
	0.450	0.10	1.00 0.20	2.92 0.60	3.96 0.96	5.21 1.11	4.53 1.04	2.73 0.82	3.22 0.66	3.60 0.75	0.34 0.19
	0.550	0.10	0.31 0.12	1.08 0.38	2.34 0.78	3.57 0.95	2.88 0.87	2.15 0.76	1.14 0.40	1.58 0.57	0.0 0.0
	0.650	0.10	0.36 0.13	0.84 0.34	0.55 0.39	0.54 0.38	2.55 0.85	0.87 0.50	0.63 0.32	0.33 0.23	0.0 0.0
	0.800	0.20	0.09 0.05	0.65 0.23	0.31 0.22	1.42 0.47	0.31 0.22	0.62 0.31	0.57 0.22	0.08 0.08	0.0 0.0
	1.000	0.20	0.0 0.0	0.08 0.08	0.17 0.17	0.49 0.28	0.17 0.17	0.50 0.29	0.0 0.0	0.0 0.0	0.0 0.0
	1.200	0.20	0.0 0.0	0.0 0.0	0.0 0.0	0.0 0.0	0.0 0.0	0.0 0.0	0.0 0.0	0.0 0.0	0.0 0.0
4.7	0.005	0.01	5.47 ± 0.85	42.86 ± 3.09	87.28 ± 4.75	123.56 ± 5.67	88.30 ± 5.82	68.52 ± 6.21	59.21 ± 4.99	62.29 ± 6.26	43.13 ± 5.08
	0.015	0.01	5.91 0.90	49.63 3.45	90.71 5.25	125.41 6.15	84.08 5.89	67.04 6.28	54.67 4.82	61.50 6.28	39.68 4.85
	0.025	0.01	7.26 0.98	39.13 3.11	79.94 5.18	99.71 5.80	90.65 6.25	69.62 6.46	68.57 5.52	59.99 6.21	30.91 4.27
	0.035	0.01	4.70 0.83	43.16 3.37	91.83 5.81	92.49 5.67	72.99 5.83	77.31 6.54	65.99 5.45	58.49 6.12	31.95 4.37
	0.045	0.01	4.44 0.77	47.40 3.59	75.75 5.51	79.11 5.62	79.41 6.26	74.48 6.88	52.81 4.88	49.29 5.68	29.89 4.25
	0.055	0.01	5.19 0.90	37.13 3.20	60.22 5.06	80.38 5.89	74.50 6.23	68.24 6.67	58.14 5.18	41.34 5.18	23.85 3.74
	0.065	0.01	3.47 0.71	32.64 3.12	62.33 5.33	74.37 5.82	63.68 5.83	66.83 6.73	45.49 4.62	34.50 5.04	20.36 3.46
	0.075	0.01	3.74 0.73	25.71 2.77	53.56 5.07	55.56 5.14	72.17 6.32	69.10 6.53	49.43 4.61	46.10 5.49	24.53 3.85
	0.085	0.01	3.72 0.71	20.49 2.50	41.57 4.58	62.74 5.59	62.50 6.03	52.32 6.10	42.12 4.52	35.03 4.78	19.78 3.51
	0.095	0.01	2.84 0.67	26.80 2.92	51.33 5.19	54.10 5.34	58.10 5.91	54.55 6.36	39.80 4.40	40.74 5.24	14.76 2.90
	0.110	0.02	3.73 0.54	22.63 1.95	40.30 3.34	49.62 3.70	56.48 4.22	53.06 4.46	44.53 3.31	32.00 3.31	20.24 2.46
	0.130	0.02	2.92 0.49	16.13 1.68	28.34 2.91	43.[illegible] 3.58	42.42 3.74	38.79 3.89	38.52 3.14	33.40 3.39	11.37 1.88
	0.150	0.02	2.36 0.43	16.31 1.73	34.75 3.30	36.09 3.37	42.63 3.87	36.08 3.81	29.21 2.76	22.38 2.78	12.60 1.95
	0.170	0.02	1.86 0.40	16.83 1.79	27.05 2.99	28.24 3.07	28.10 3.21	33.56 3.73	27.50 2.70	27.55 3.13	10.15 1.75
	0.190	0.02	2.29 0.45	14.39 1.68	26.20 3.03	23.28 2.85	24.14 3.02	31.36 3.70	21.13 2.39	20.08 2.65	10.82 1.81
	0.225	0.05	1.56 0.23	9.76 0.90	17.92 1.64	20.02 1.74	20.13 1.80	21.46 1.98	18.97 1.45	13.29 1.40	5.83 0.85
	0.275	0.05	1.06 0.20	7.60 0.83	14.86 1.57	12.78 1.45	11.30 1.40	16.39 1.78	14.87 1.32	12.56 1.37	4.70 0.76
	0.325	0.05	1.05 0.20	5.65 0.74	5.74 1.31	10.98 1.39	12.69 1.54	9.44 1.39	8.53 1.01	7.23 1.05	2.48 0.56
	0.375	0.05	0.85 0.18	5.46 0.74	7.71 1.21	8.53 1.27	6.54 1.14	8.64 1.38	6.66 0.92	4.38 0.83	1.82 0.49
	0.450	0.10	0.75 0.12	3.08 0.41	3.79 0.62	5.09 0.73	4.75 0.72	5.72 0.81	4.58 0.55	3.80 0.56	0.97 0.25
	0.550	0.10	0.48 0.10	2.32 0.37	2.52 0.54	3.65 0.65	2.91 0.58	2.77 0.59	2.98 0.45	2.22 0.44	0.33 0.15
	0.650	0.10	0.20 0.07	1.48 0.31	1.97 0.49	2.01 0.50	1.79 0.48	1.85 0.49	1.65 0.35	1.58 0.37	0.42 0.17
	0.800	0.20	0.06 0.03	0.69 0.15	0.47 0.18	0.95 0.26	0.63 0.21	1.09 0.28	0.71 0.17	0.64 0.17	0.03 0.03
	1.000	0.20	0.04 0.02	0.20 0.09	0.08 0.08	0.38 0.17	0.15 0.11	0.16 0.11	0.52 0.15	0.34 0.13	0.0 0.0
	1.200	0.20	0.0 0.0	0.09 0.06	0.17 0.12	0.16 0.12	0.09 0.09	0.0 0.0	0.05 0.05	0.10 0.07	0.0 0.0
	1.400	0.20	0.0 0.0	0.14 0.08	0.0 0.0	0.18 0.13	0.18 0.12	0.10 0.10	0.0 0.0	0.0 0.0	0.0 0.0
	1.600	0.20	0.0 0.0	0.0 0.0	0.0 0.0	0.0 0.0	0.0 0.0	0.10 0.10	0.0 0.0	0.0 0.0	0.0 0.0
9.3	0.005	0.01	3.66 ± 0.71	39.90 ± 3.06	131.39 ± 4.70	133.84 ± 5.40	92.43 ± 5.49	78.20 ± 6.83	61.40 ± 5.24	55.84 ± 6.23	49.30 ± 5.69
	0.015	0.01	3.60 0.72	39.36 3.02	99.14 4.55	128.50 5.21	98.22 6.29	63.40 6.20	56.07 5.07	42.97 5.40	23.23 3.84
	0.025	0.01	4.00 0.77	35.51 3.09	84.12 4.80	111.04 5.56	95.46 6.44	74.61 6.82	56.14 5.13	50.36 5.52	30.16 4.33
	0.035	0.01	2.04 0.56	37.01 3.05	85.11 5.01	100.39 5.60	90.65 6.29	69.72 6.66	53.82 5.06	42.68 5.45	28.69 4.20
	0.045	0.01	3.13 0.67	27.34 2.66	80.78 5.08	91.92 5.48	88.70 6.33	68.14 6.65	58.26 5.30	42.26 5.43	18.20 3.39
	0.055	0.01	2.71 0.64	25.83 2.55	70.62 4.90	95.84 5.72	81.73 6.20	68.96 6.73	52.82 5.02	46.24 5.68	19.90 3.59
	0.065	0.01	2.43 0.60	24.12 2.51	66.41 4.87	74.32 5.17	65.97 5.67	66.06 6.71	47.75 4.82	35.50 5.00	18.98 3.42
	0.075	0.01	1.53 0.47	23.82 2.50	58.19 4.67	70.10 5.15	61.29 5.49	72.06 6.96	40.90 4.53	33.83 4.85	24.13 3.93
	0.085	0.01	1.58 0.49	25.14 2.65	51.54 4.50	68.44 5.23	54.19 5.28	57.95 6.31	45.57 4.72	27.42 4.41	14.91 3.06
	0.095	0.01	2.66 0.62	22.11 2.54	48.57 4.48	57.64 4.85	56.59 5.42	45.41 5.57	45.51 4.68	34.59 4.96	14.09 2.95
	0.110	0.02	1.18 0.28	17.67 1.61	41.27 3.00	59.14 3.59	56.72 3.91	44.51 3.95	46.75 3.40	35.56 3.55	10.62 1.80
	0.130	0.02	2.59 0.45	14.73 1.51	37.57 2.95	47.79 3.35	42.92 3.48	44.95 4.05	35.57 3.01	18.09 2.54	9.46 1.74
	0.150	0.02	2.37 0.44	1[illegible].60 1.57	30.37 2.77	33.26 2.47	33.45 3.13	33.93 3.55	33.77 2.94	23.20 2.89	12.08 1.94
	0.170	0.02	1.08 0.29	14.64 1.55	27.11 2.66	26.97 2.62	29.82 3.02	34.91 3.65	28.37 2.70	20.65 2.74	8.27 1.63
	0.190	0.02	2.33 0.42	12.00 1.45	20.56 2.38	28.34 2.78	20.42 2.54	29.94 3.42	22.67 2.45	18.77 2.61	4.70 1.22
	0.225	0.05	0.92 0.17	9.35 0.92	20.47 1.54	21.36 1.58	22.76 1.75	21.52 1.97	19.53 1.44	15.70 1.52	5.06 0.79
	0.275	0.05	0.96 0.17	7.57 0.77	13.15 1.29	16.16 1.44	15.44 1.50	15.01 1.60	13.41 1.22	11.95 1.32	3.50 0.66
	0.325	0.05	0.69 0.15	6.17 0.70	8.79 1.10	10.15 1.18	10.83 1.20	12.51 1.54	10.10 1.07	6.73 1.01	2.13 0.52
	0.375	0.05	0.84 0.18	5.25 0.67	8.54 1.12	9.46 1.18	9.98 1.27	7.60 1.19	7.37 0.93	4.10 0.79	2.07 0.52
	0.450	0.10	0.73 0.12	3.59 0.40	4.57 0.61	6.59 0.73	7.53 0.90	6.76 0.91	5.01 0.55	3.41 0.52	1.64 0.33
	0.550	0.10	0.56 0.10	2.67 0.36	4.17 0.60	3.62 0.57	4.22 0.63	4.76 0.70	2.70 0.41	3.10 0.49	0.93 0.25
	0.650	0.10	0.25 0.07	0.89 0.22	2.06 0.44	2.13 0.45	2.30 0.48	3.74 0.64	2.11 0.37	1.65 0.37	0.52 0.19
	0.800	0.20	1.10 0.03	0.91 0.16	0.90 0.22	1.31 0.26	1.30 0.24	1.54 0.30	1.22 0.21	0.76 0.18	0.20 0.08
	1.000	0.20	0.07 0.03	0.29 0.09	0.40 0.15	0.57 0.18	0.71 0.21	0.70 0.21	0.62 0.15	0.26 0.10	0.10 0.06
	1.200	0.20	0.01 0.01	0.13 0.07	0.63 0.20	0.0 0.0	0.26 0.13	0.21 0.12	0.24 0.10	0.36 0.13	0.11 0.06
	1.400	0.20	0.0 0.0	0.11 0.06	0.07 0.07	0.41 0.17	0.07 0.07	0.07 0.07	0.28 0.11	0.0 0.0	0.07 0.05
	1.600	0.20	0.01 0.01	0.04 0.04	0.14 0.10	0.0 0.0	0.0 0.0	0.08 0.08	0.0 0.0	0.05 0.05	0.0 0.0
	1.800	0.20	0.0 0.0	0.0 0.0	0.0 0.0	0.0 0.0	0.0 0.0	0.0 0.0	0.18 0.09	0.05 0.05	0.0 0.0
	2.000	0.20	0.01 0.01	0.0 0.0	0.0 0.0	0.0 0.0	0.0 0.0	0.0 0.0	0.0 0.0	0.0 0.0	0.0 0.0

1986C33

FIGURE CAPTIONS

1. a) Scatter plot of π^- longitudinal momentum $p_{\parallel}$ in the laboratory frame and $x = p^*_{\parallel}/p^*_{max}$ in the c.m.s. for the 9.3 GeV data.

   b) Scatter plot of π^- longitudinal momentum $p_{\parallel}$ and the rapidity $y = \frac{1}{2} \ln\left[(E+p_{\parallel})/(E-p_{\parallel})\right]$ in the laboratory frame.

   c) Scatter plot of $y = \frac{1}{2} \ln\left[(E+p_{\parallel})/(E-p_{\parallel})\right]$ and $x = p^*_{\parallel}/p^*_{max}$. The curves in each case show contours of constant transverse momentum calculated for $E\gamma = 9.3$ GeV.

2. Photon energy spectra for the exposures at (a) 2.8, (b) 4.7, and (c) 9.3 GeV.

3. Total and topological photoproduction cross sections versus the center-of-mass energy squared s. The lines are provided only to help distinguish between topologies.

4. Structure function $\mathscr{F}(p_{\parallel})$ in the laboratory at 2.8, 4.7, and 9.3 GeV for $\gamma p \rightarrow \pi^- + \text{(anything)}$. The insert shows the region $p_{\parallel} < 300$ MeV on an expanded scale. Data given in Table IV.

5. Structure function $\mathscr{F}(p_{\perp}^2)$ for $-0.15 < p_{\parallel}$ (LAB) < 0.15 GeV at 2.8, 4.7, and 9.3 GeV.

6. Structure function $\mathscr{F}(p_{\parallel}, s)$ in the laboratory for labelled intervals in $p_{\parallel}$ versus $s^{-1/2}$.

7. Longitudinal-momentum distributions $d\sigma/dp_{\parallel}$ in the laboratory system normalized to the total cross sections at $s=\infty$ for hadron-induced reactions compared with our photoproduction results at 9.3 GeV. Curves are polynomial fits to the hadron-induced data with representative data points shown (as provided by the authors quoted).

8. Sketch of the general features of the "rapidity" variable distribution $d\sigma/dy$ for secondary particles as predicted by the multiperipheral model. The labels I, II, and III correspond to the target, central, and beam regions, respectively, discussed in the text.

9. $\gamma p \to \pi^-$ (anything) at 9.3 GeV: Scatter plot of the rapidity variable y in the laboratory frame versus transverse momentum squared $p_\perp^2$.

10. Reaction $\gamma p \to \pi^-$ + (anything): Differential π^- cross section $d\sigma/dy$. The solid and broken bell-shaped curves superimposed on the 9.3 GeV data represent the 2.8 and 4.7 GeV data beneath, having the same y_{min} while the partial curves are the lower energy data transposed to have the same y_{max}. Data given in Table V.

11. Reaction $\gamma p \to \pi^-$ + (anything): Differential π^- cross section $d\sigma/dy$ for various intervals in the transverse momentum at 2.8, 4.7, and 9.3 GeV.

12. Reaction $\gamma p \to \pi^-$ + (anything): Structure function F(x) for $E_\gamma = 2.8$, 4.7 and 9.3 GeV. Data given in Table VI.

13. The structure function F(x, s) integrated over different intervals in x plotted as functions of s.

14. Normalized structure function $F(x)/\sigma_{TOT}(\infty)$ for photoproduced π^- reactions compared with those for $\pi^\pm$ induced reactions (Ref. 17). Curves are approximations to the hadron-induced data with representative data points shown.

15. F(x) with the elastic ρ^0 events excluded ($\gamma p \to \pi^+\pi^- p$ with $M_{\pi^+\pi^-} < 1.0$ GeV removed), for a) 2.8 GeV, b) 4.7 GeV, c) 9.3 GeV, above each we show the contribution to F(x) from the ρ^0. d) F(x) for the 4.7 and 9.3 GeV data superimposed for comparison for $x < 0$. e) same for $x > 0$.

16. F(x) for 3, 5, 7, 9-prong events separately at 9.3 GeV. The curves show the contributions from the events having no missing neutrals, a single π^o missing, a single neutron missing and from multineutral events.

17. The structure function $F(x, \langle p_\perp^2 \rangle)$ plotted versus x for various intervals in transverse momentum. Data given in Table VII.

18. Structure function $f_3(x, p_\perp^2)$ at 9.3 GeV a) for finite x-intervals b) same data for selected x-intervals shown on an expanded scale. Data given in Table VIII.

19. $F(\langle x \rangle, p_\perp^2)$ for 3, 5, 7, 9- prong events separately at 9.3 GeV. The curves are the results of fits to $F(\langle x \rangle, 0) \exp(-Ap_\perp^2)$ for $p_\perp^2 < 0.3\ (\mathrm{GeV}/c)^2$. See Table I for values of A.

20. Average charged-prong multiplicity (labelled $\langle n \rangle$) and π^- (labelled $\langle n^- \rangle$) versus s. The straight lines are the results of a fit of the data to the form $\langle n \rangle = c\, \ln s + d$ ($c = 0.93 \pm 0.12$, $d = 1.01 \pm 0.22$) and ($c^- = 0.44 \pm 0.04$, $d^- = 0.07 \pm 0.08$).

21. Dominant diagram expected to contribute to π^- production near the kinematic boundaries for a) target associated π^-, b) beam associated π^-.

22. Values of the effective Regge trajectory, determined as described in the text, as a function of t for a) target vertex, b) photon vertex. The curve corresponds to the Δ trajectory.

23. The differential cross section $d\sigma/d\phi$ plotted against the azimuthal angle ϕ between the outgoing pion and the polarization vector of the photon, for various x-intervals. Elastic ρ^o production is not included in the ϕ points and is given separately by the ϕ points. Data are at 9.3 GeV.

24. The longitudinal momentum $p_{\parallel}$ distributions at 9.3 GeV in the frame where $R = p_{proton}/p_{photon}$ has the value a) $R = 1.0$ (c.m.s. frame), b) $R = 1.5$ (Q-system), and c) $R = 2.3$ (symmetric frame). Elastic ρ^{o} production events have been excluded.

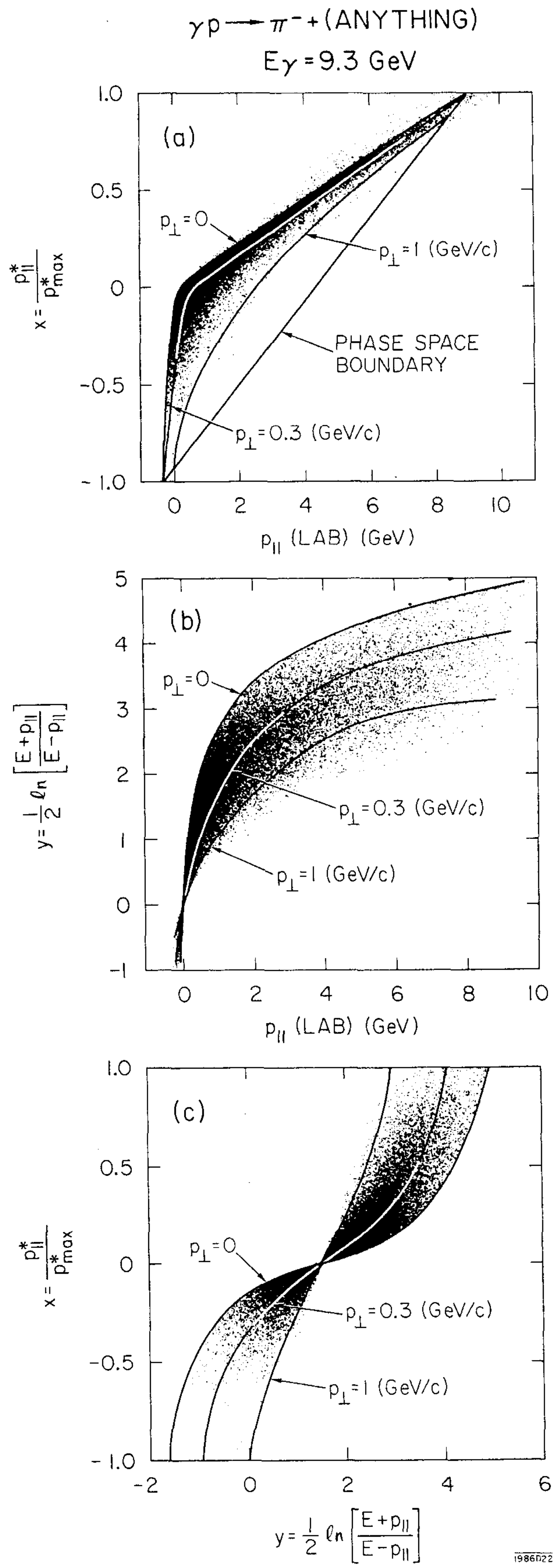

γp → π⁻ + (ANYTHING)
Eγ = 9.3 GeV
(a)
(b)
(c)
$p_\perp = 0$
$p_\perp = 0.3$ (GeV/c)
$p_\perp = 1$ (GeV/c)
PHASE SPACE BOUNDARY
$x = \frac{p^*_\parallel}{p^*_{max}}$
$p_\parallel$ (LAB) (GeV)
$y = \frac{1}{2} \ell n \left[\frac{E+p_\parallel}{E-p_\parallel}\right]$
1986D22

Fig. 1

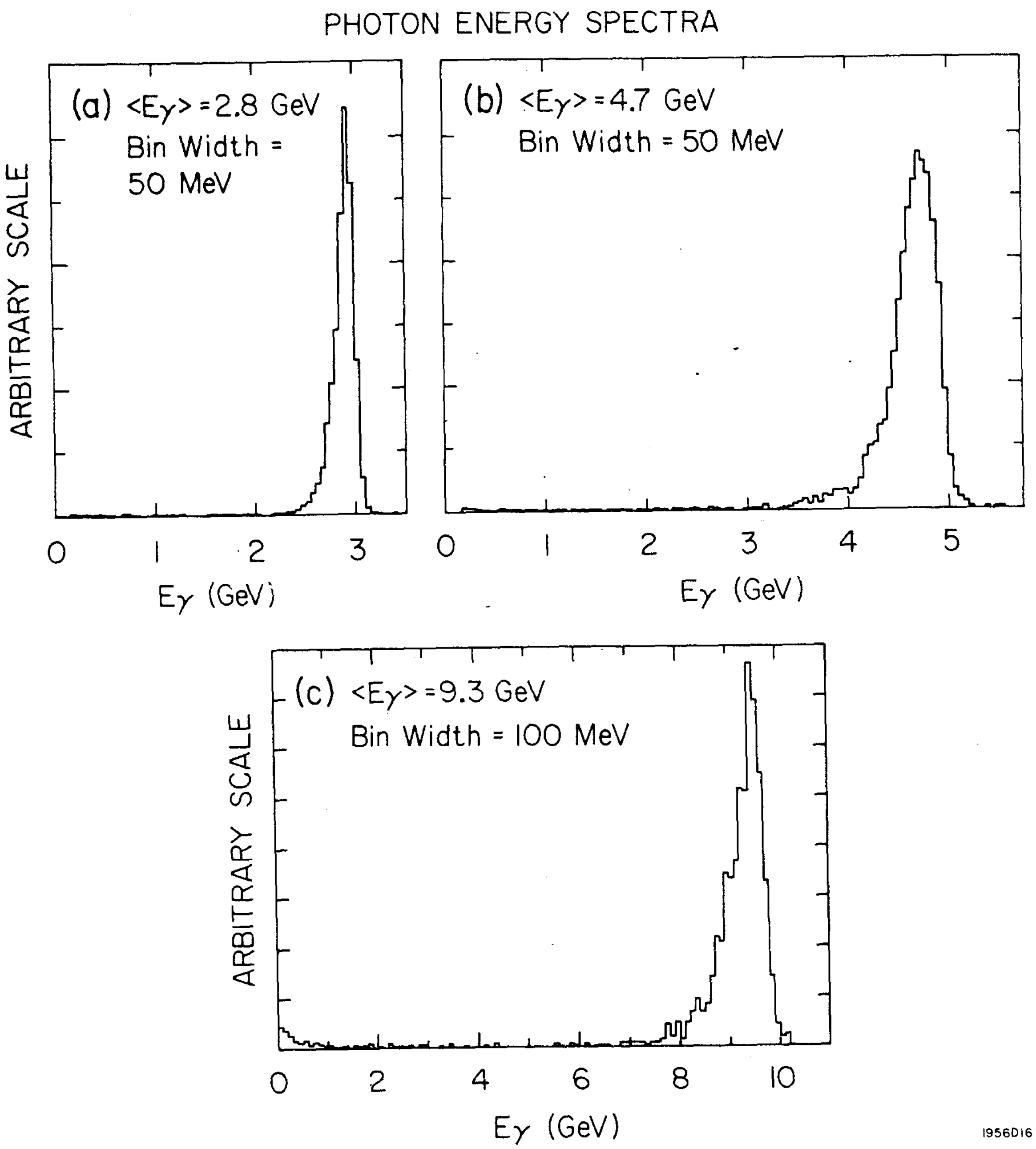

PHOTON ENERGY SPECTRA
(a) <Eγ> =2.8 GeV
Bin Width =
50 MeV
ARBITRARY SCALE
0 1 2 3
Eγ (GeV)
(b) <Eγ> =4.7 GeV
Bin Width = 50 MeV
0 1 2 3 4 5
Eγ (GeV)
(c) <Eγ> =9.3 GeV
Bin Width = 100 MeV
ARBITRARY SCALE
0 2 4 6 8 10
Eγ (GeV)
1956D16

Fig. 2

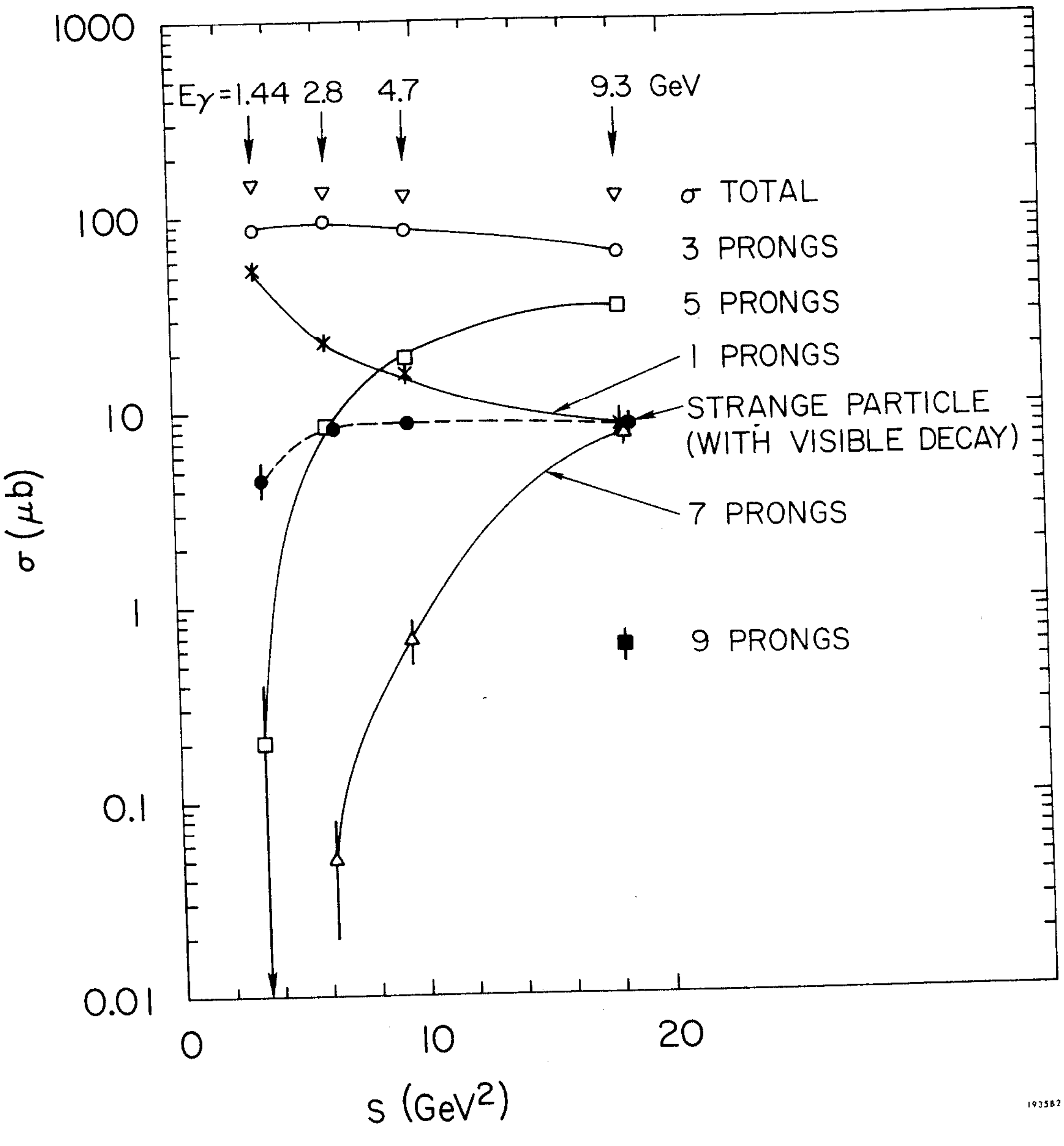
1000
100
10
1
0.1
0.01
σ (μb)
0
10
20
s (GeV^2)
Eγ=1.44 2.8 4.7 9.3 GeV
σ TOTAL
3 PRONGS
5 PRONGS
1 PRONGS
STRANGE PARTICLE (WITH VISIBLE DECAY)
7 PRONGS
9 PRONGS

Fig. 3

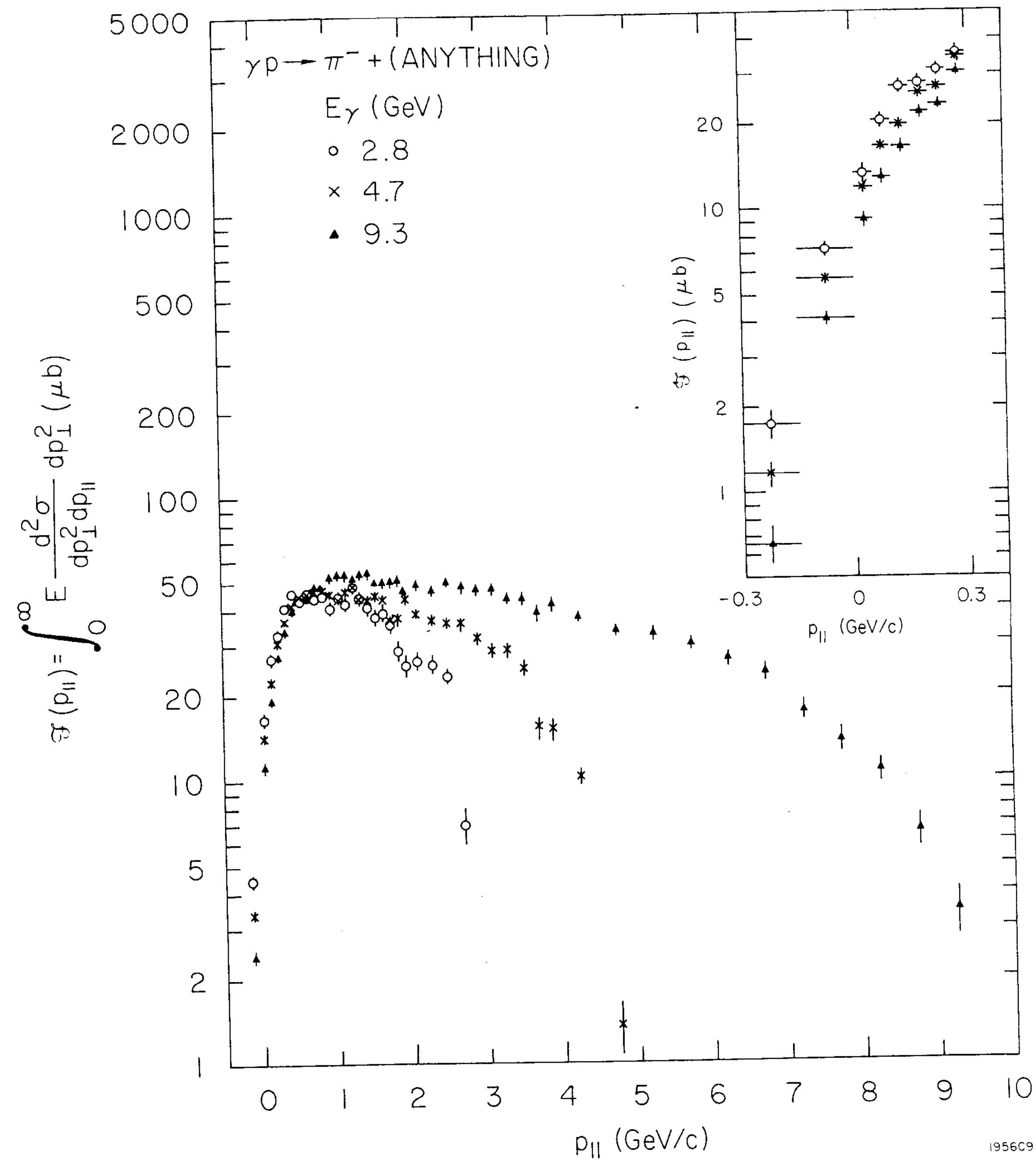

γp → π⁻ + (ANYTHING)
Eγ (GeV)
○ 2.8
× 4.7
▲ 9.3
5000
2000
1000
500
200
100
50
20
10
5
2
1
0
1
2
3
4
5
6
7
8
9
10
p∥ (GeV/c)
𝔉(p∥) = ∫₀^∞ E d²σ/(dp⊥² dp∥) dp⊥² (μb)
𝔉(p∥) (μb)
-0.3
0
0.3
1956C9

Fig. 4

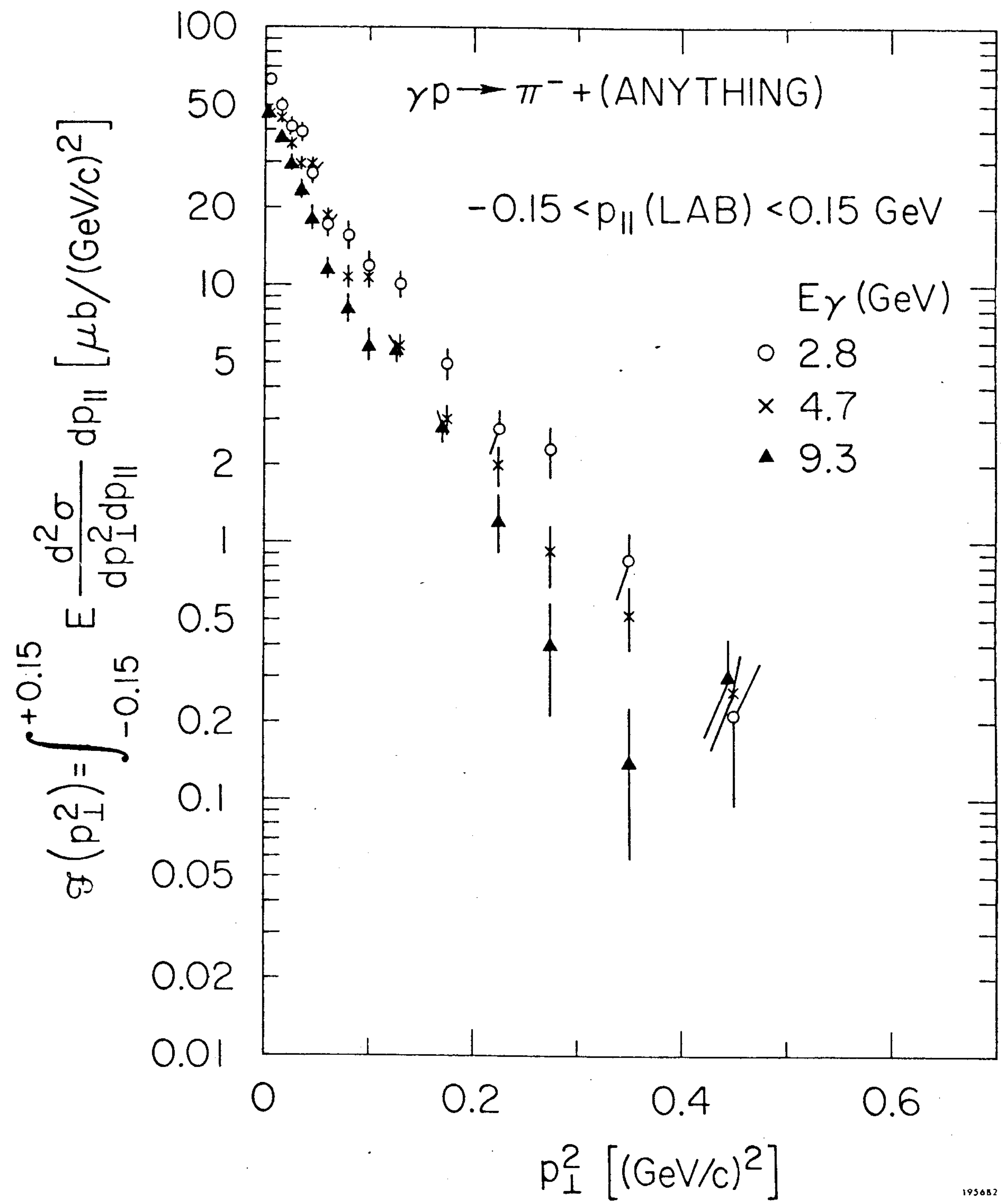
γp → π⁻ + (ANYTHING)
−0.15 < p∥ (LAB) < 0.15 GeV
Eγ (GeV)
2.8
4.7
9.3
σ(p⊥²) = ∫₋₀.₁₅^{+0.15} E d²σ/(dp⊥² dp∥) dp∥ [μb/(GeV/c)²]
p⊥² [(GeV/c)²]
100
50
20
10
5
2
1
0.5
0.2
0.1
0.05
0.02
0.01
0
0.2
0.4
0.6
195682

Fig. 5

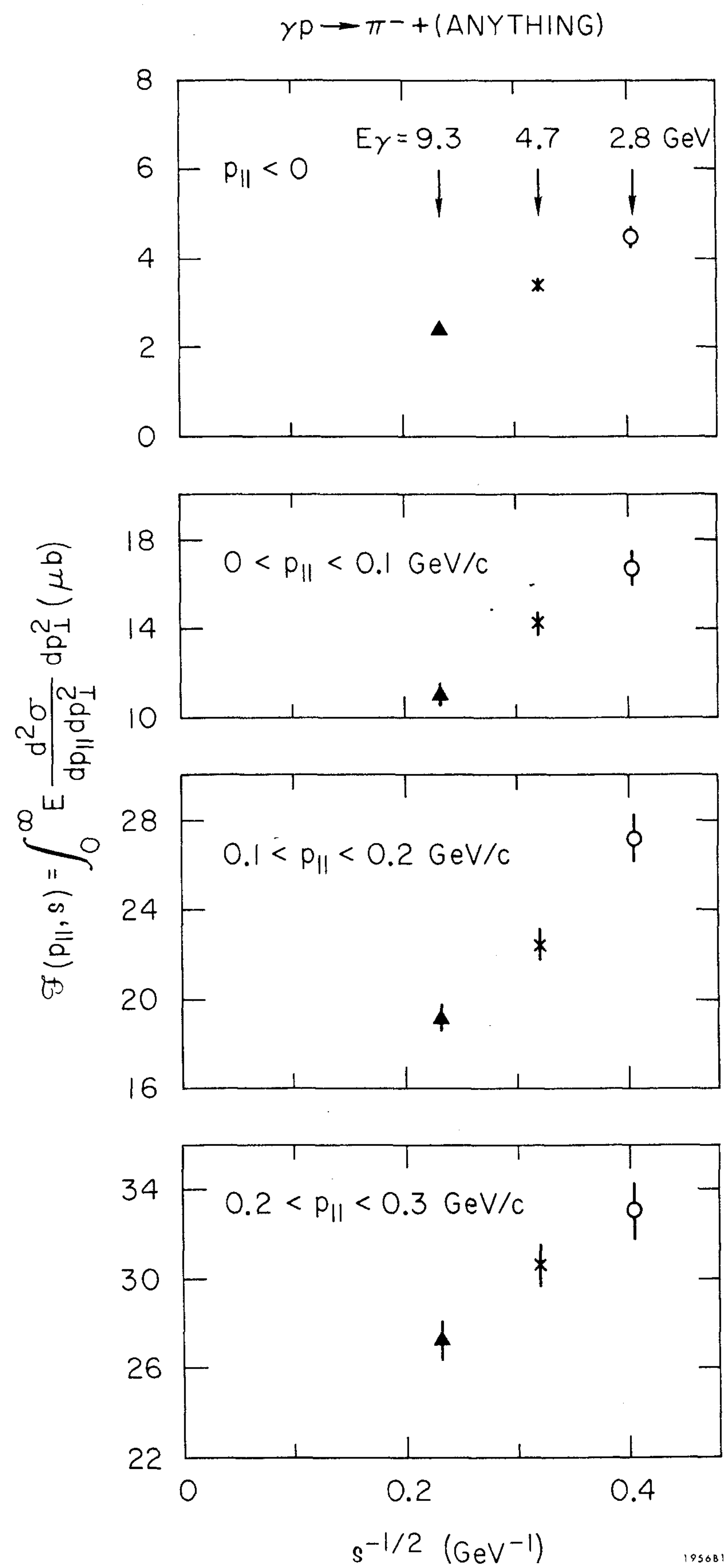

$\gamma p \rightarrow \pi^- + (\text{ANYTHING})$
$E\gamma = 9.3$
4.7
2.8 GeV
$p_{\parallel} < 0$
$0 < p_{\parallel} < 0.1$ GeV/c
$0.1 < p_{\parallel} < 0.2$ GeV/c
$0.2 < p_{\parallel} < 0.3$ GeV/c
$\mathcal{F}(p_{\parallel}, s) = \int_0^\infty E \frac{d^2\sigma}{dp_{\parallel} dp_{\perp}^2} dp_{\perp}^2 \, (\mu b)$
$s^{-1/2}$ (GeV^{-1})
0
0.2
0.4
0
2
4
6
8
10
14
18
16
20
24
28
22
26
30
34
195681

Fig. 6

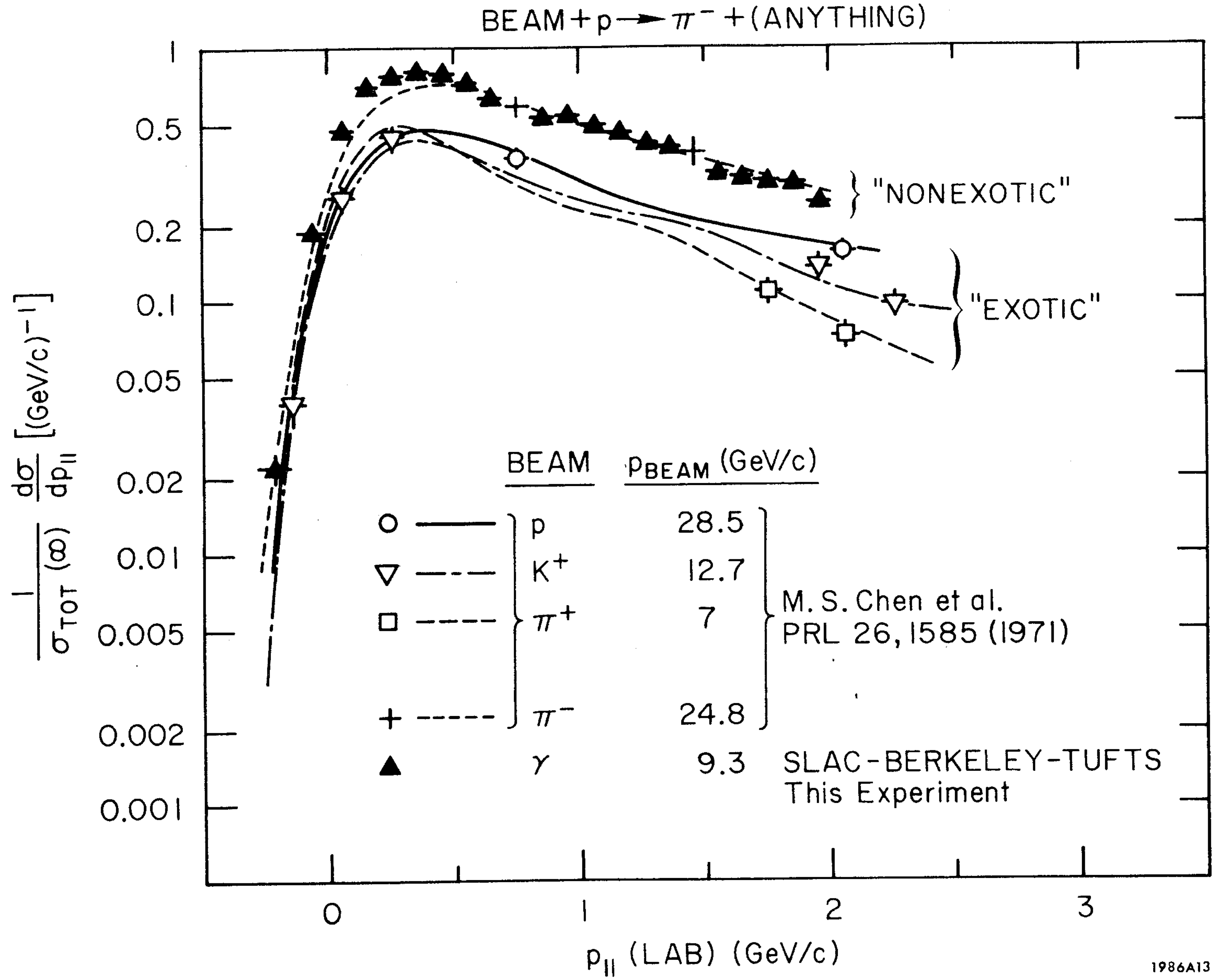

BEAM+p → π^- +(ANYTHING)
"NONEXOTIC"
"EXOTIC"
$\frac{1}{\sigma_{TOT}(\infty)} \frac{d\sigma}{dp_{\parallel}}$ [(GeV/c)$^{-1}$]
1
0.5
0.2
0.1
0.05
0.02
0.01
0.005
0.002
0.001
0
1
2
3
$p_{\parallel}$ (LAB) (GeV/c)
BEAM
p_{BEAM} (GeV/c)
p 28.5
K^+ 12.7
π^+ 7
π^- 24.8
M. S. Chen et al.
PRL 26, 1585 (1971)
γ 9.3
SLAC-BERKELEY-TUFTS
This Experiment
1986A13

Fig. 7

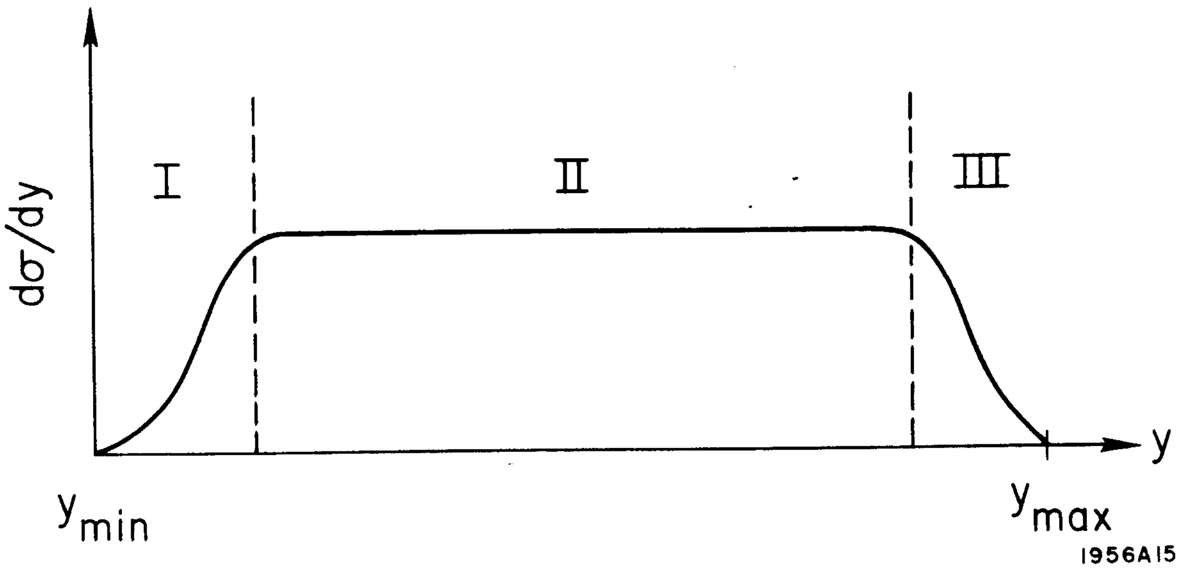

Fig. 8

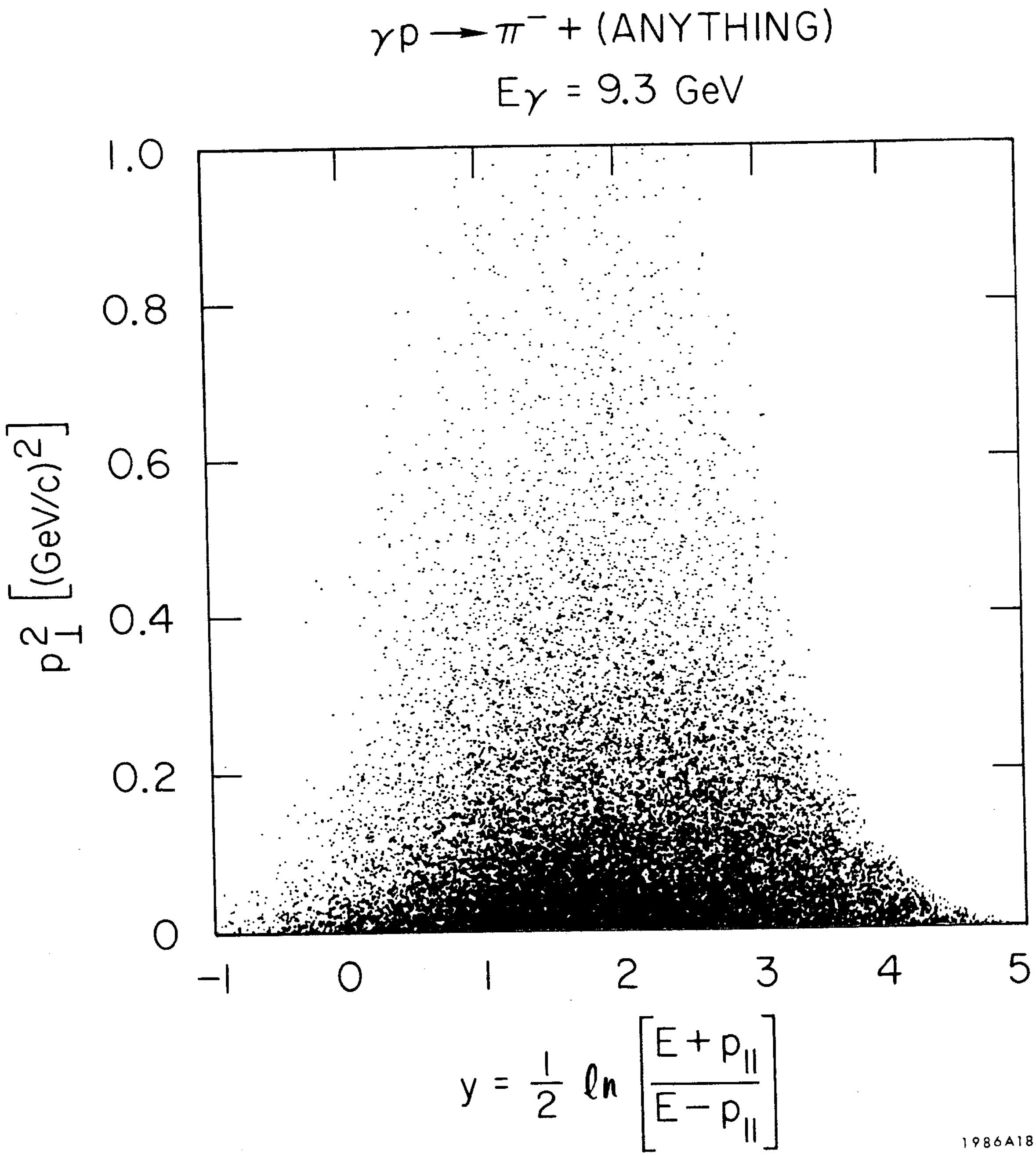
$\gamma p \rightarrow \pi^- +$ (ANYTHING)
E_γ = 9.3 GeV
1.0
0.8
0.6
0.4
0.2
0
$p_\perp^2$ [(GeV/c)^2]
−1
0
1
2
3
4
5
$y = \frac{1}{2} \ln \left[\frac{E+p_{\parallel}}{E-p_{\parallel}}\right]$
1986A18

Fig. 9

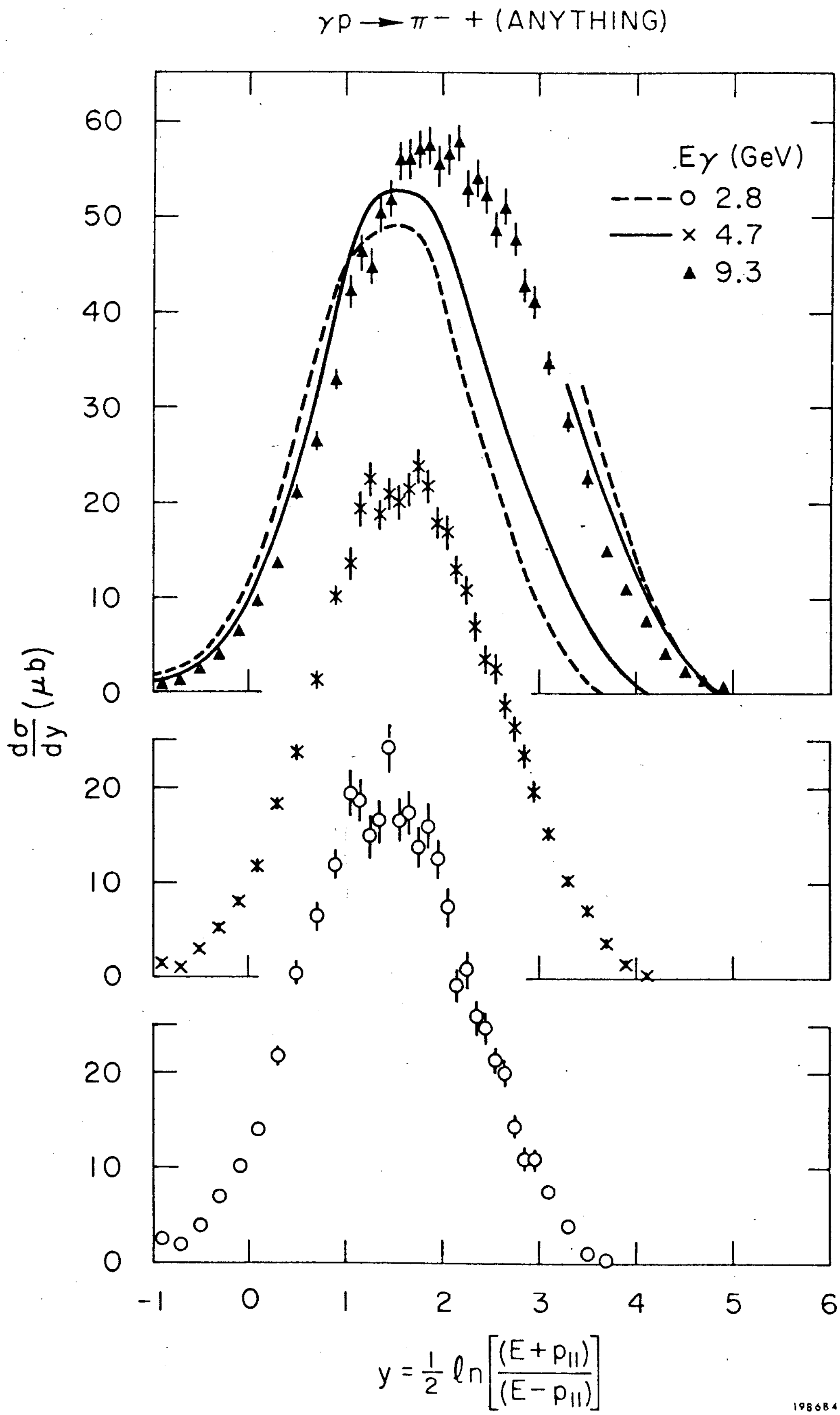

$\gamma p \rightarrow \pi^- +$ (ANYTHING)
$E\gamma$ (GeV)
2.8
4.7
9.3
$\frac{d\sigma}{dy}$ (μb)
60
50
40
30
20
10
0
-1
0
1
2
3
4
5
6
$y = \frac{1}{2} \ln \left[\frac{(E+p_{\parallel})}{(E-p_{\parallel})} \right]$
1986B4

Fig. 10

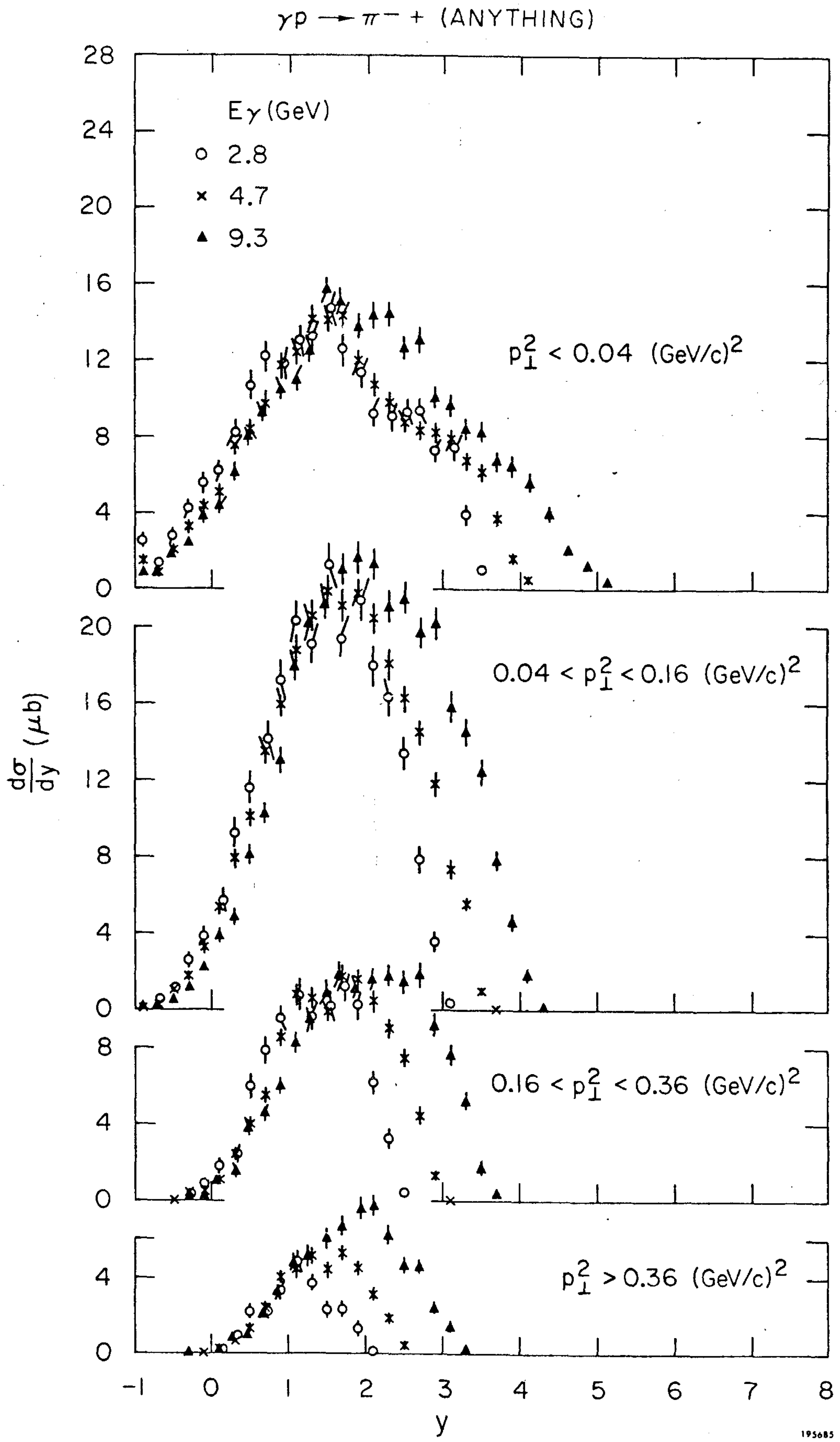
γp → π⁻ + (ANYTHING)
Eγ (GeV)
2.8
4.7
9.3
p⊥² < 0.04 (GeV/c)²
0.04 < p⊥² < 0.16 (GeV/c)²
0.16 < p⊥² < 0.36 (GeV/c)²
p⊥² > 0.36 (GeV/c)²
dσ/dy (μb)
y
1956B5

Fig. 11

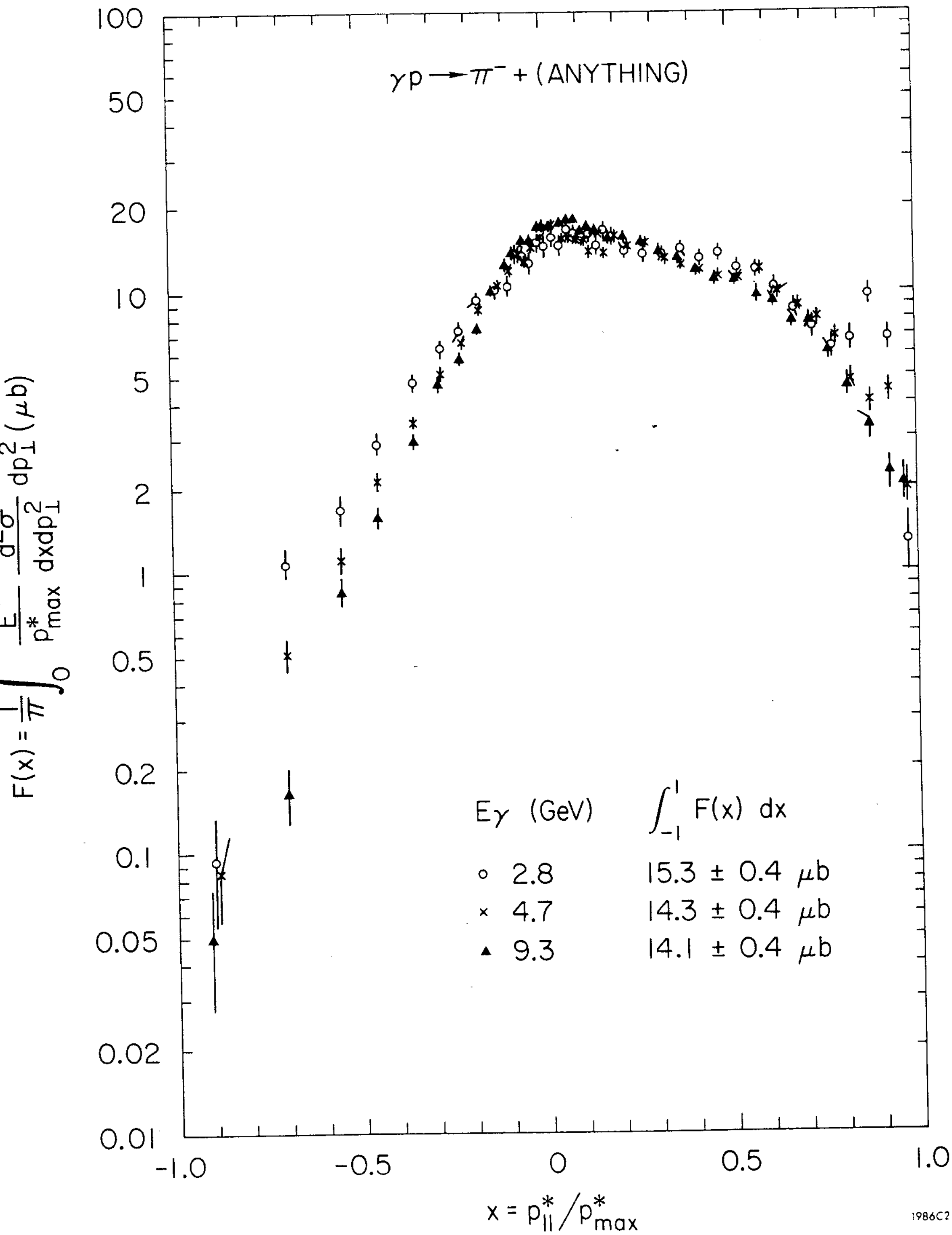

$\gamma p \to \pi^- +$ (ANYTHING)
$F(x) = \frac{1}{\pi}\int_0^\infty \frac{E^*}{p^*_{max}} \frac{d^2\sigma}{dx\,dp_\perp^2} dp_\perp^2$ (μb)
$x = p^*_{\parallel}/p^*_{max}$
$E\gamma$ (GeV) $\int_{-1}^{1} F(x)\, dx$
○ 2.8 15.3 ± 0.4 μb
× 4.7 14.3 ± 0.4 μb
▲ 9.3 14.1 ± 0.4 μb
100
50
20
10
5
2
1
0.5
0.2
0.1
0.05
0.02
0.01
-1.0
-0.5
0
0.5
1.0
1986C2

Fig. 12

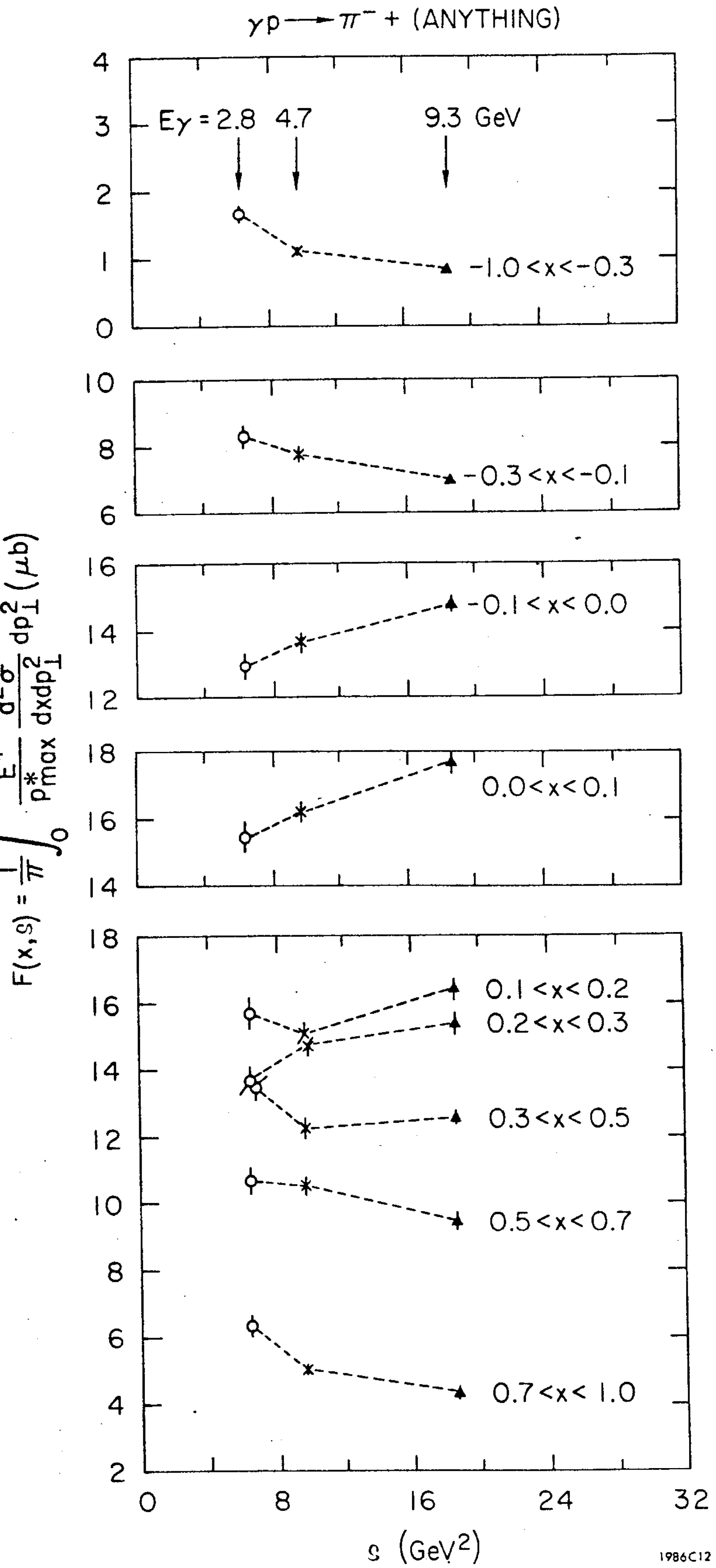
γp ⟶ π⁻ + (ANYTHING)
Eγ = 2.8
4.7
9.3 GeV
−1.0 < x < −0.3
−0.3 < x < −0.1
−0.1 < x < 0.0
0.0 < x < 0.1
0.1 < x < 0.2
0.2 < x < 0.3
0.3 < x < 0.5
0.5 < x < 0.7
0.7 < x < 1.0
F(x,s) = 1/π ∫₀^∞ E*/p*max d²σ/dxdp⊥² dp⊥² (μb)
s (GeV²)
1986C12

Fig. 13

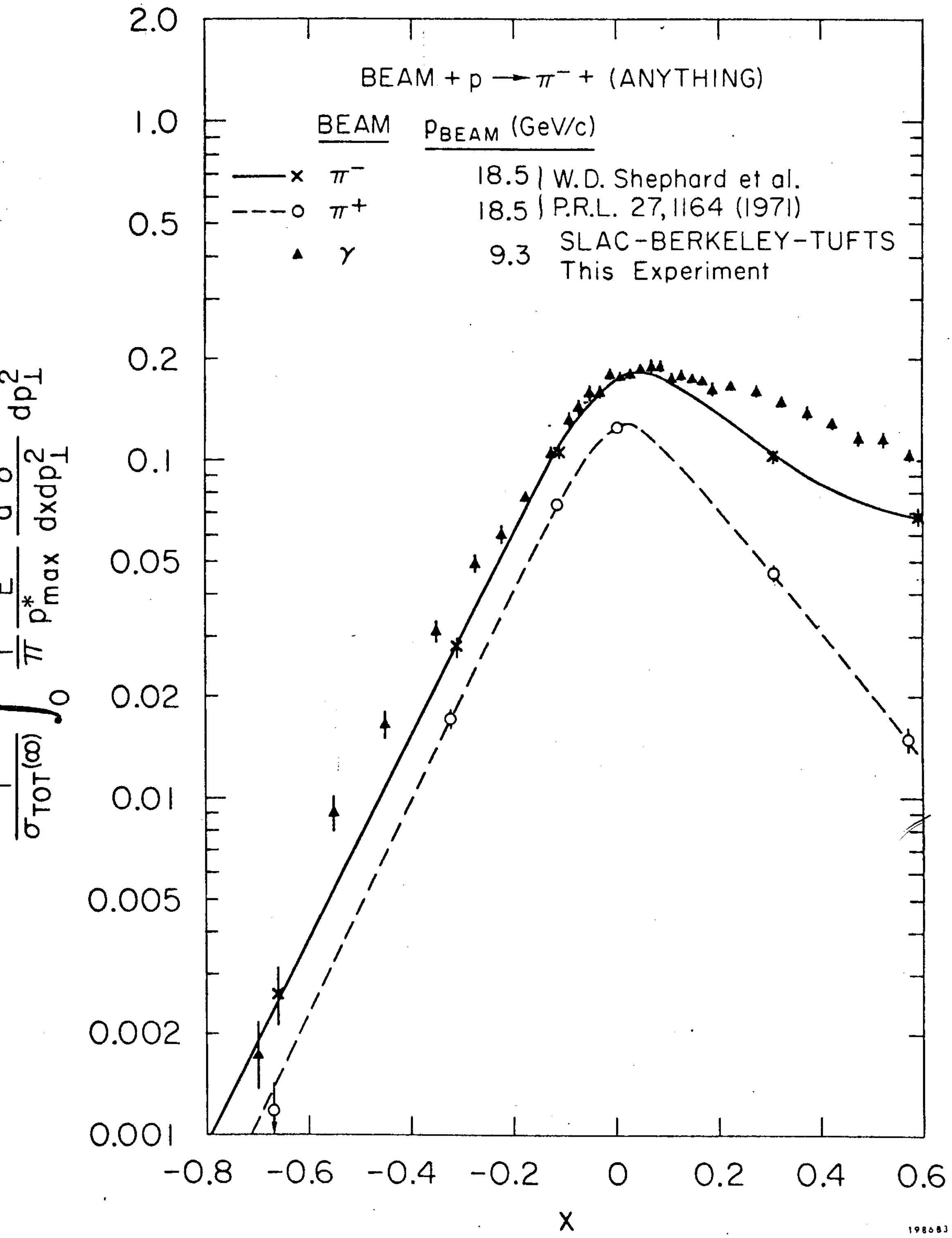

BEAM + p ⟶ π^- + (ANYTHING)
BEAM
p_{BEAM} (GeV/c)
π^- 18.5 W. D. Shephard et al.
π^+ 18.5 P.R.L. 27, 1164 (1971)
γ 9.3 SLAC-BERKELEY-TUFTS
This Experiment
$\frac{1}{\sigma_{TOT}(\infty)} \int_0^\infty \frac{1}{\pi} \frac{E^*}{p^*_{max}} \frac{d^2\sigma}{dx\,dp_\perp^2} dp_\perp^2$
2.0
1.0
0.5
0.2
0.1
0.05
0.02
0.01
0.005
0.002
0.001
−0.8
−0.6
−0.4
−0.2
0
0.2
0.4
0.6
X
198683

Fig. 14

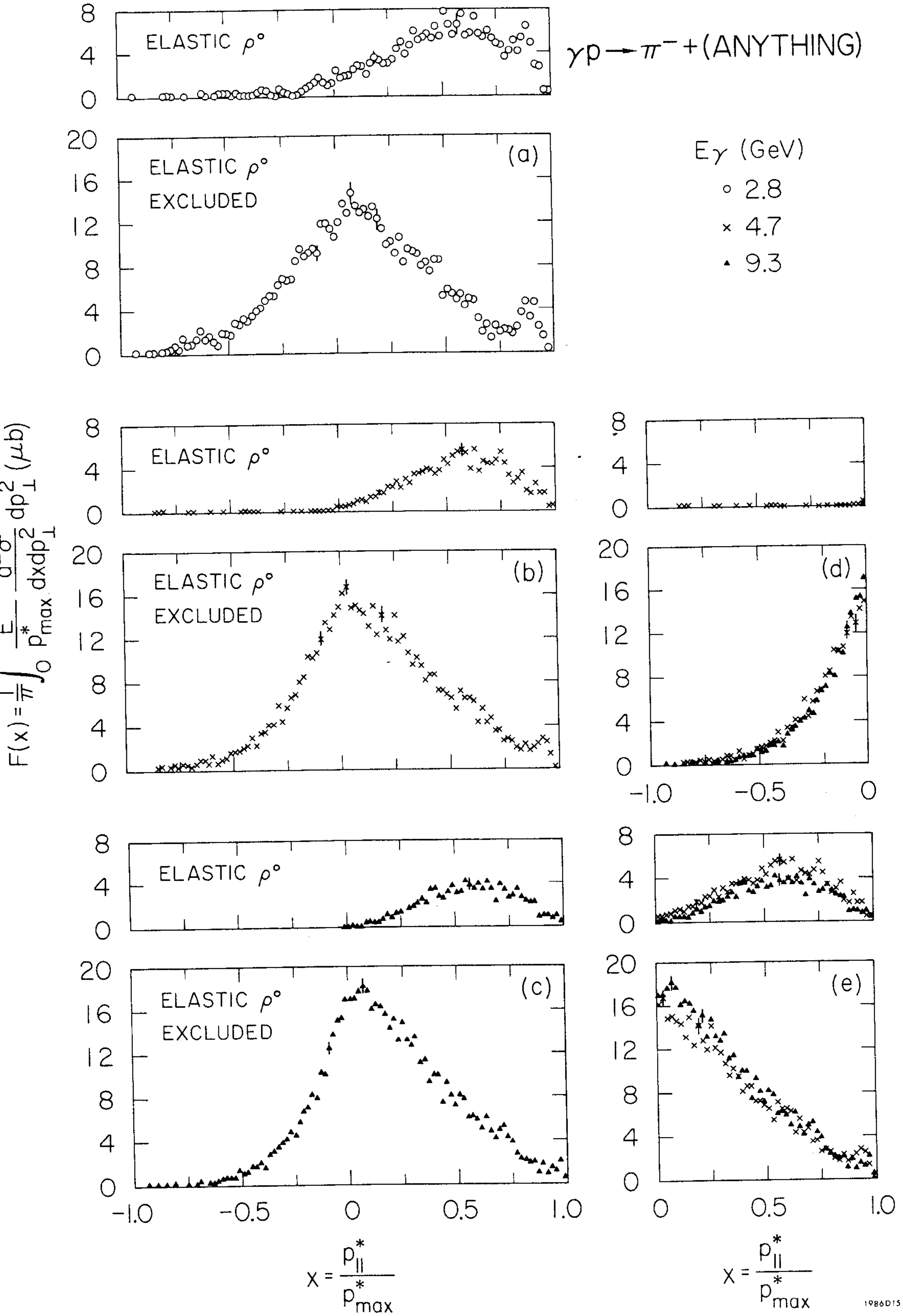

$\gamma p \to \pi^- + (\mathrm{ANYTHING})$
E_γ (GeV)
○ 2.8
× 4.7
▲ 9.3
ELASTIC ρ°
ELASTIC ρ° EXCLUDED
(a)
(b)
(c)
(d)
(e)
$F(x) = \frac{1}{\pi}\int_0^\infty \frac{E^*}{p^*_{max}} \frac{d^2\sigma}{dx\,dp_\perp^2} dp_\perp^2$ (μb)
$x = \frac{p^*_\parallel}{p^*_{max}}$
1986D15

Fig. 15

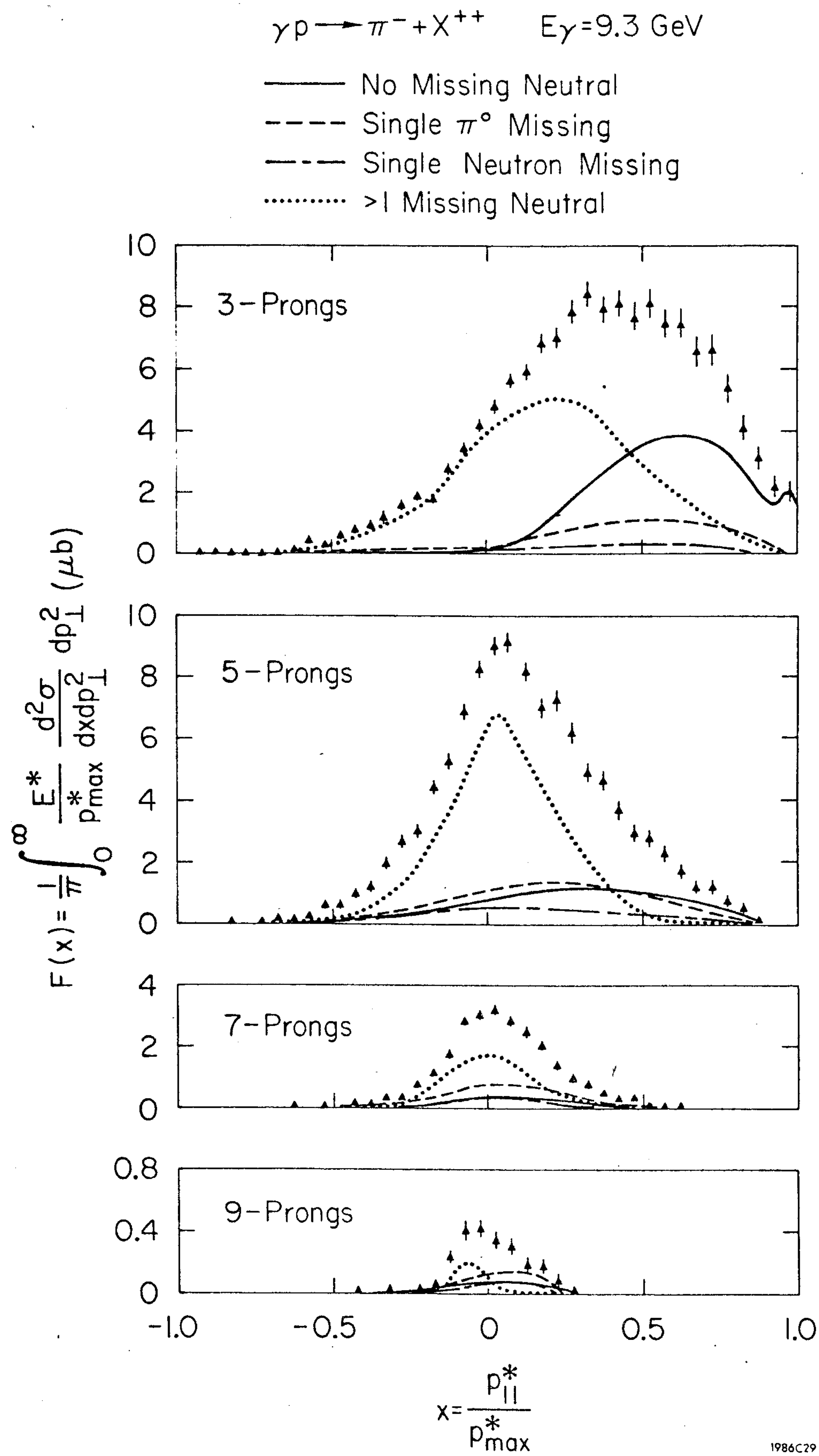
$\gamma p \rightarrow \pi^- + X^{++}$ $E\gamma = 9.3$ GeV
No Missing Neutral
Single π° Missing
Single Neutron Missing
>1 Missing Neutral
3-Prongs
5-Prongs
7-Prongs
9-Prongs
$F(x) = \frac{1}{\pi}\int_0^\infty \frac{E^*}{p^*_{max}} \frac{d^2\sigma}{dx dp_\perp^2} dp_\perp^2$ (μb)
$x = \frac{p^*_{\parallel}}{p^*_{max}}$
1986C29

Fig. 16

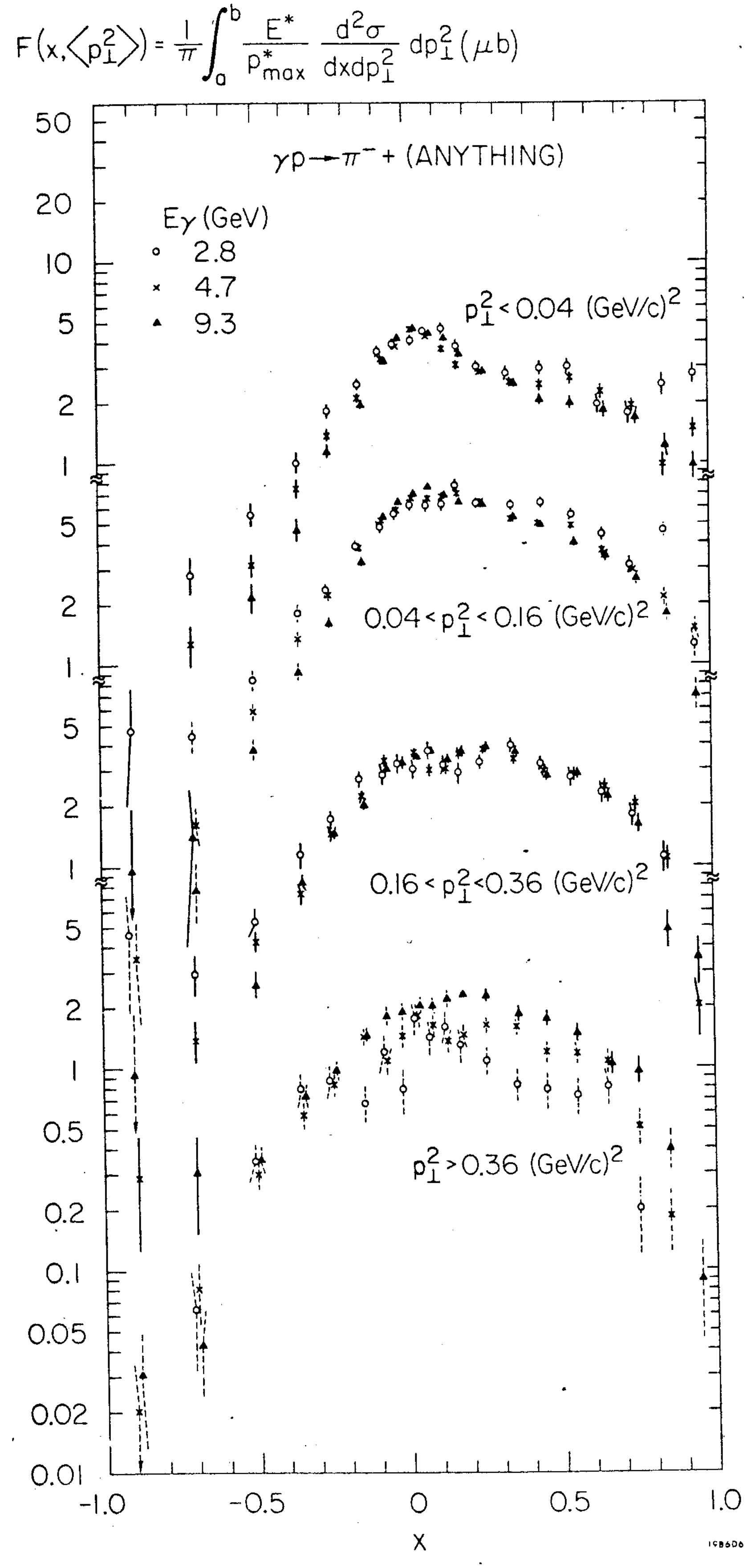
$F(x,\langle p_\perp^2\rangle) = \frac{1}{\pi}\int_a^b \frac{E^*}{p^*_{max}} \frac{d^2\sigma}{dx\,dp_\perp^2}\, dp_\perp^2\ (\mu b)$
$\gamma p \rightarrow \pi^- + $ (ANYTHING)
$E\gamma$ (GeV)
2.8
4.7
9.3
$p_\perp^2 < 0.04$ (GeV/c)^2
$0.04 < p_\perp^2 < 0.16$ (GeV/c)^2
$0.16 < p_\perp^2 < 0.36$ (GeV/c)^2
$p_\perp^2 > 0.36$ (GeV/c)^2
50
20
10
5
2
1
0.5
0.2
0.1
0.05
0.02
0.01
-1.0
-0.5
0
0.5
1.0
X

Fig. 17

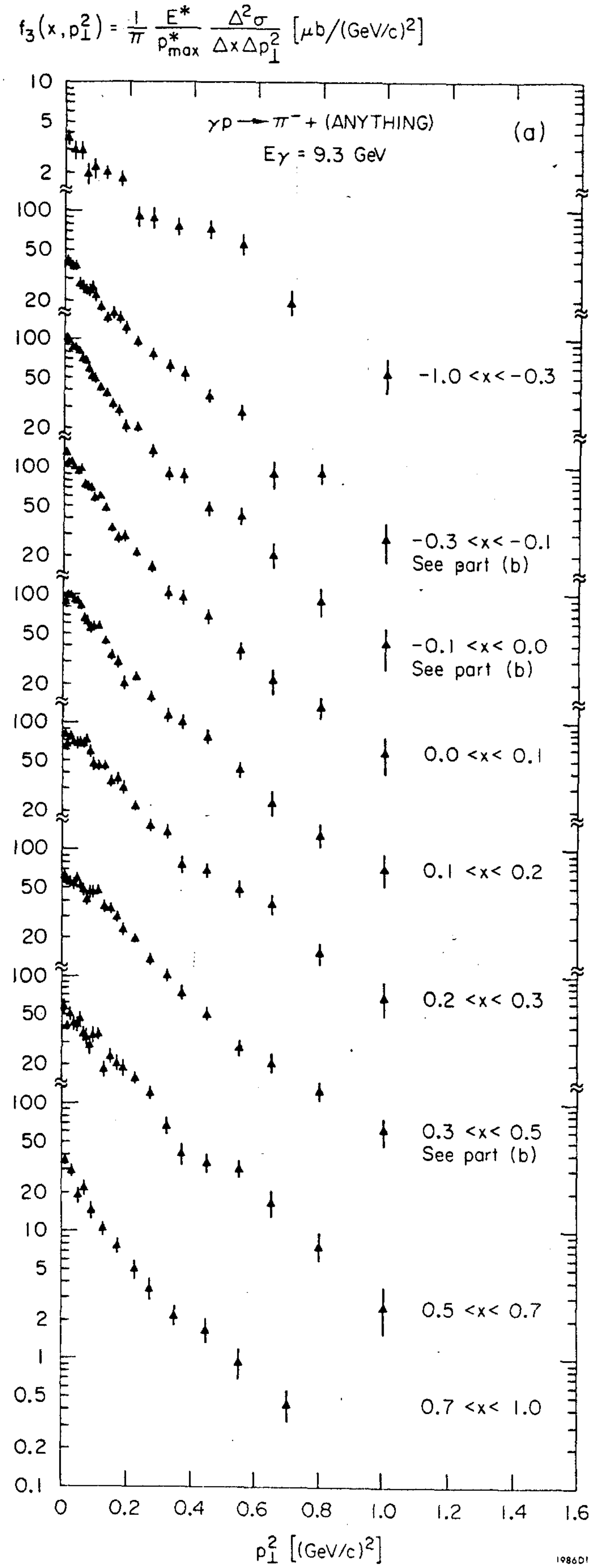

$f_3(x, p_\perp^2) = \frac{1}{\pi} \frac{E^*}{p^*_{max}} \frac{\Delta^2\sigma}{\Delta x \Delta p_\perp^2}$ $[\mu b/(GeV/c)^2]$
$\gamma p \to \pi^- + $ (ANYTHING)
$E_\gamma = 9.3$ GeV
(a)
$-1.0 < x < -0.3$
$-0.3 < x < -0.1$
See part (b)
$-0.1 < x < 0.0$
See part (b)
$0.0 < x < 0.1$
$0.1 < x < 0.2$
$0.2 < x < 0.3$
$0.3 < x < 0.5$
See part (b)
$0.5 < x < 0.7$
$0.7 < x < 1.0$
$p_\perp^2$ $[(GeV/c)^2]$
1986D1

Fig. 18A

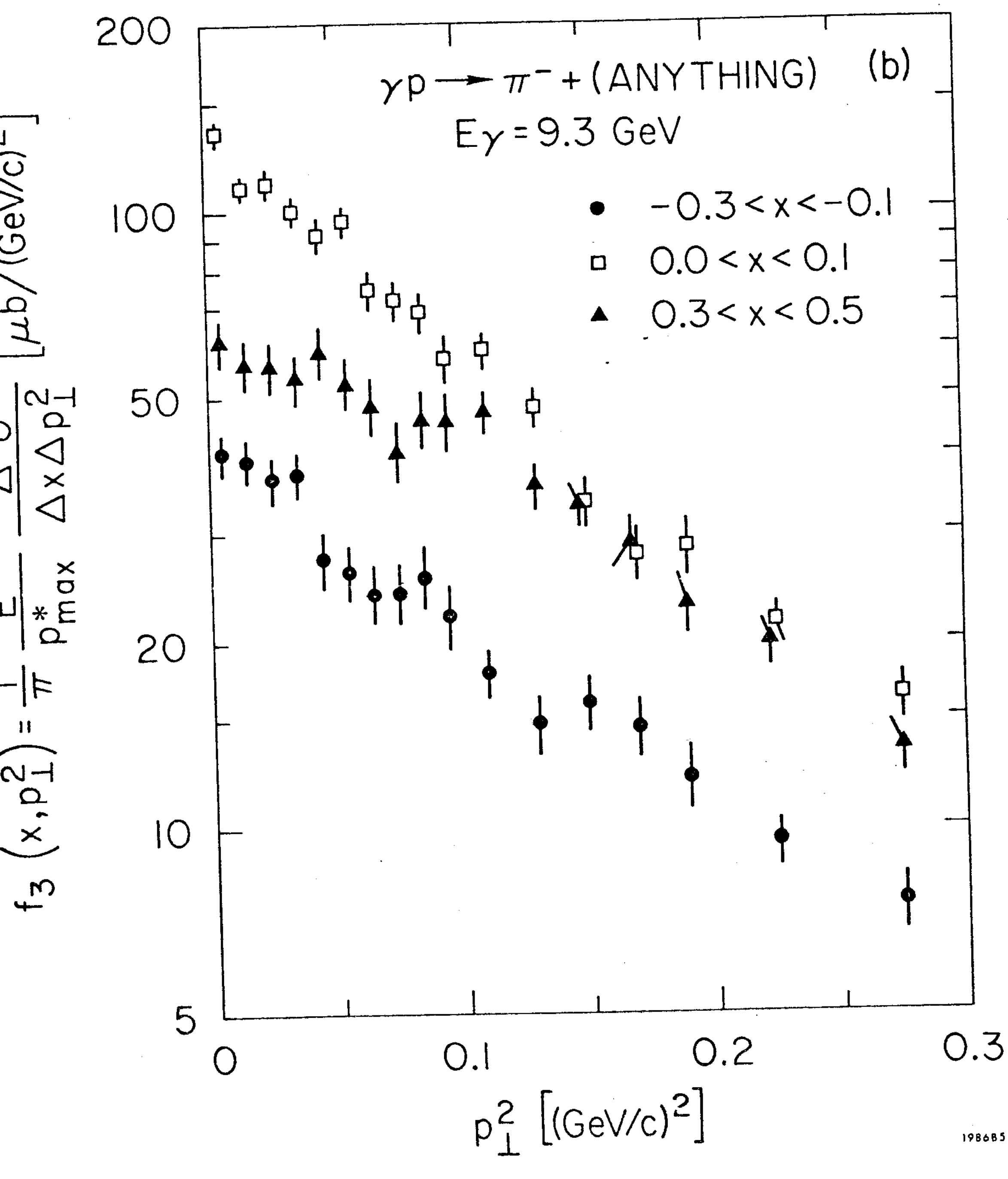

$\gamma p \rightarrow \pi^- + (\mathrm{ANYTHING})$
(b)
$E\gamma = 9.3$ GeV
$-0.3 < x < -0.1$
$0.0 < x < 0.1$
$0.3 < x < 0.5$
$f_3(x, p_\perp^2) = \frac{1}{\pi} \frac{E^*}{p^*_{max}} \frac{\Delta^2\sigma}{\Delta x \Delta p_\perp^2}$ $[\mu b/(\mathrm{GeV}/c)^2]$
$p_\perp^2$ $[(\mathrm{GeV}/c)^2]$
200
100
50
20
10
5
0
0.1
0.2
0.3
1986B5

Fig. 18B

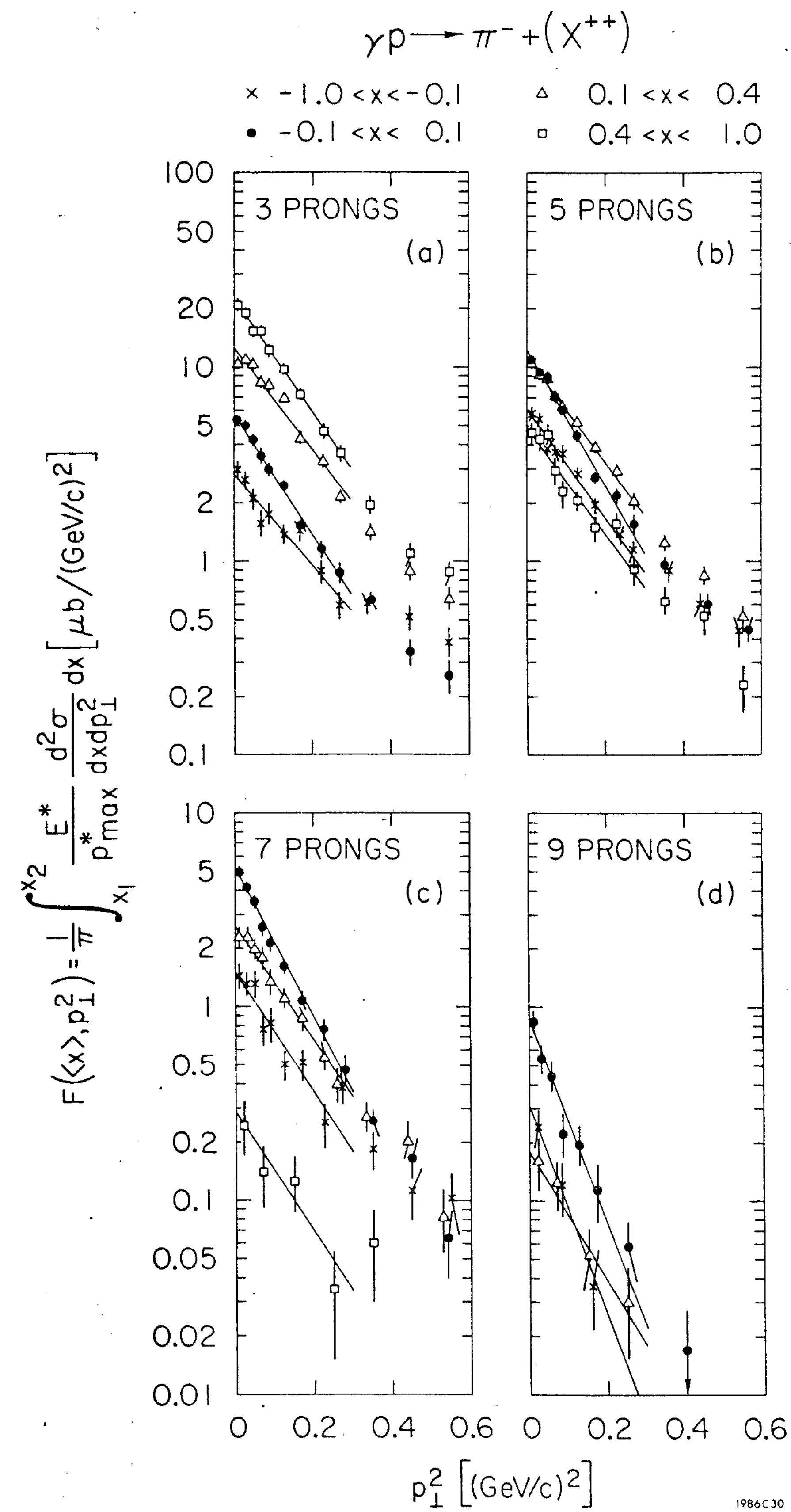

$\gamma p \to \pi^- + (X^{++})$
× −1.0 < x < −0.1
• −0.1 < x < 0.1
△ 0.1 < x < 0.4
□ 0.4 < x < 1.0
3 PRONGS
(a)
5 PRONGS
(b)
7 PRONGS
(c)
9 PRONGS
(d)
$F(\langle x\rangle, p_\perp^2) = \frac{1}{\pi}\int_{x_1}^{x_2} \frac{E^*}{p^*_{max}} \frac{d^2\sigma}{dx\,dp_\perp^2} dx \left[\mu b/(GeV/c)^2\right]$
$p_\perp^2 \left[(GeV/c)^2\right]$
1986C30

Fig. 19

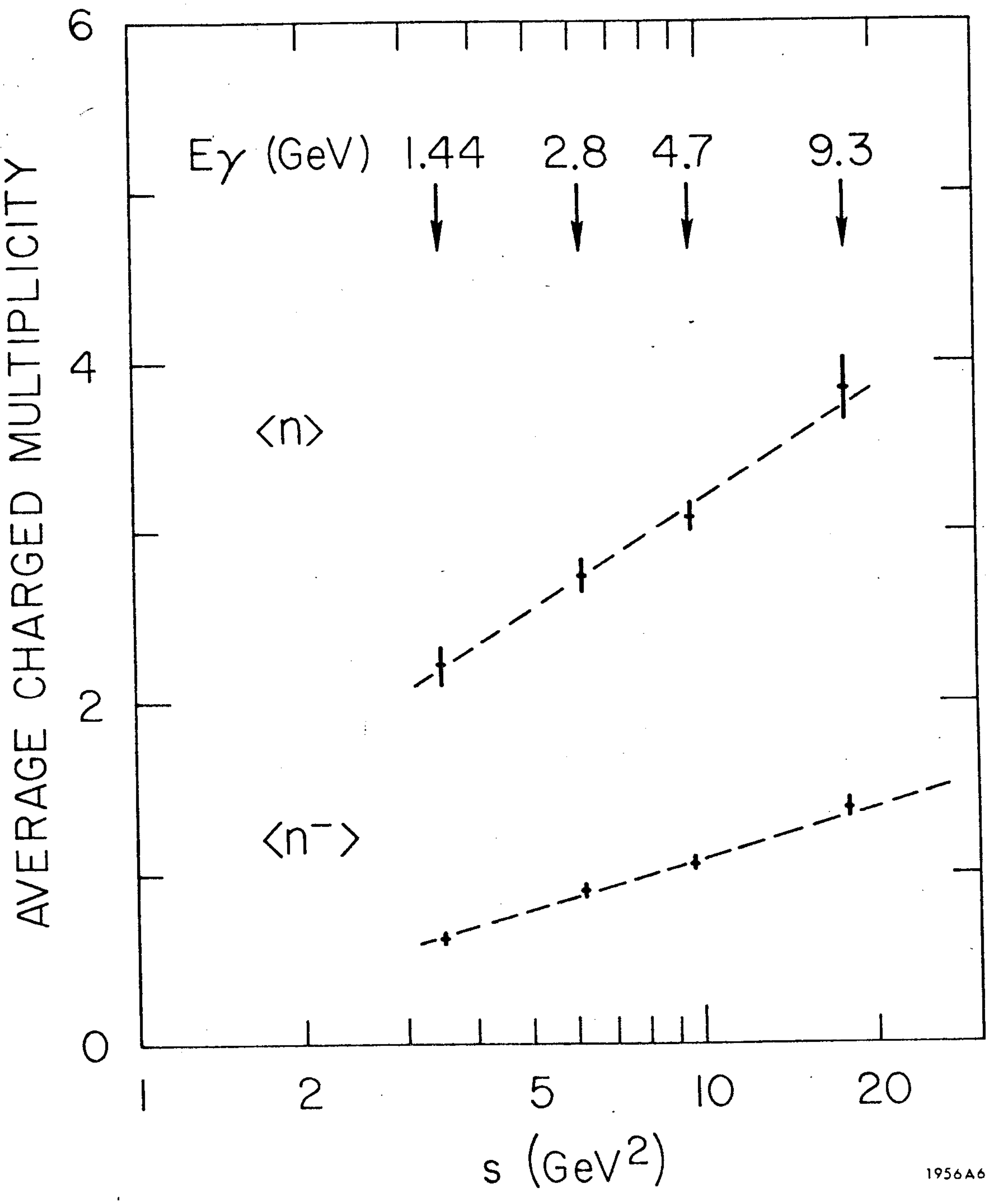
AVERAGE CHARGED MULTIPLICITY
Eγ (GeV) 1.44 2.8 4.7 9.3
⟨n⟩
⟨n⁻⟩
6
4
2
0
1
2
5
10
20
s (GeV²)
1956A6

Fig. 20

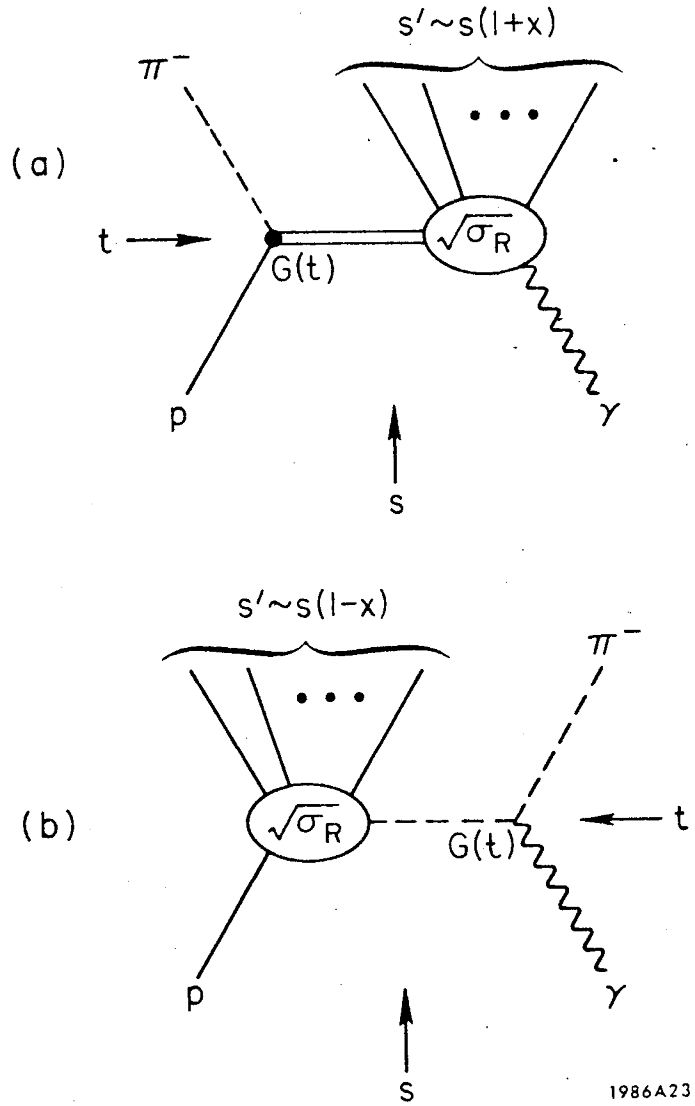

Fig. 21

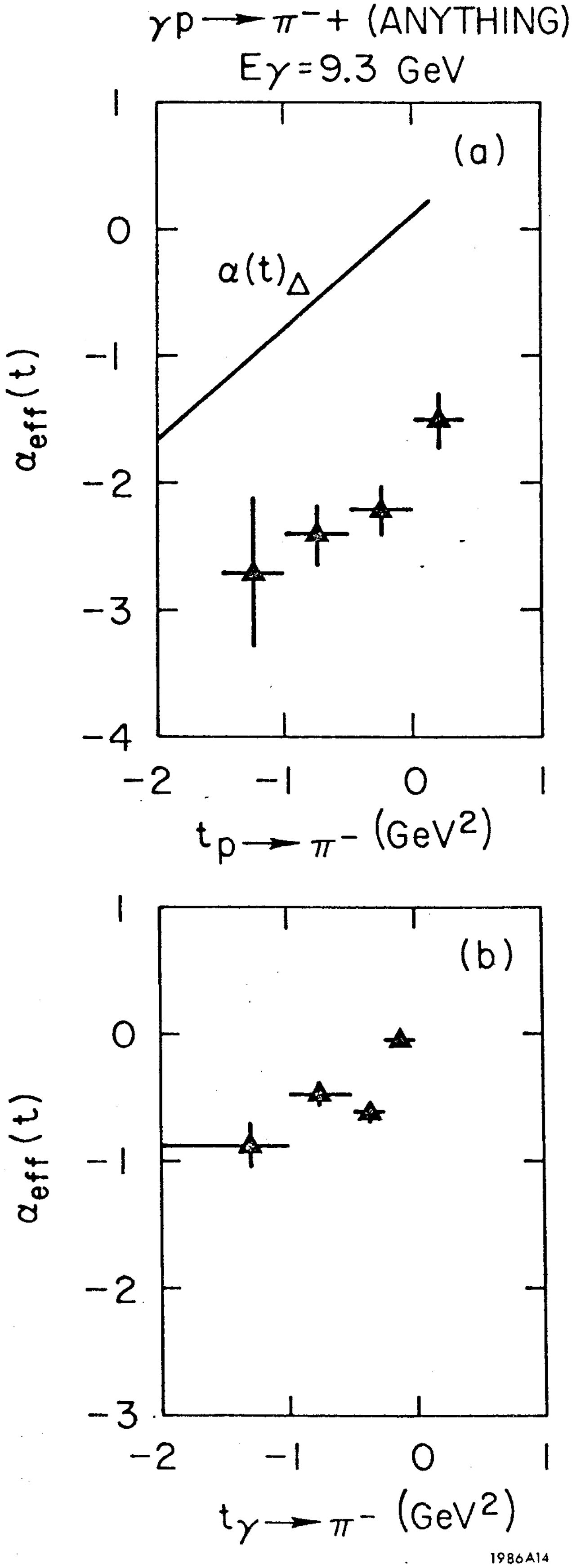

$\gamma p \rightarrow \pi^- +$ (ANYTHING)
$E\gamma = 9.3$ GeV
(a)
$\alpha(t)_\Delta$
$\alpha_{eff}(t)$
$t_{p \rightarrow \pi^-}$ (GeV^2)
(b)
$\alpha_{eff}(t)$
$t_{\gamma \rightarrow \pi^-}$ (GeV^2)
1986A14

Fig. 22

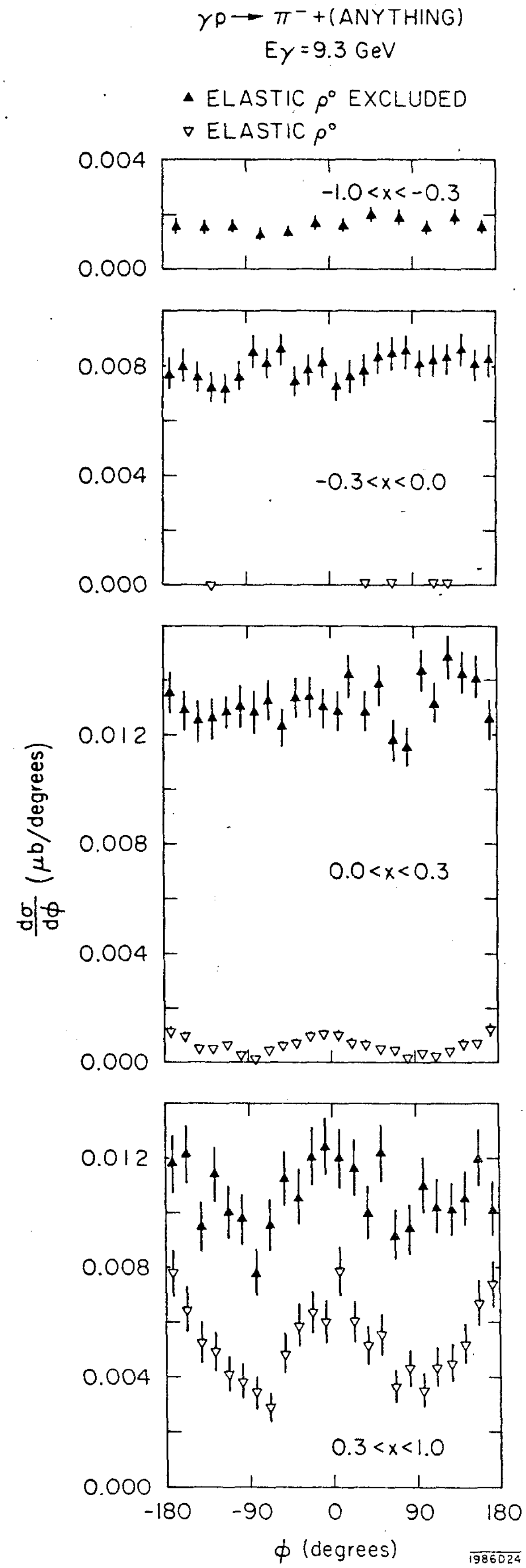

γp → π⁻ + (ANYTHING)
Eγ = 9.3 GeV
▲ ELASTIC ρ° EXCLUDED
▽ ELASTIC ρ°
-1.0 < x < -0.3
-0.3 < x < 0.0
0.0 < x < 0.3
0.3 < x < 1.0
dσ/dφ (μb/degrees)
φ (degrees)
0.000
0.004
0.008
0.012
-180
-90
0
90
180
1986D24

Fig. 23

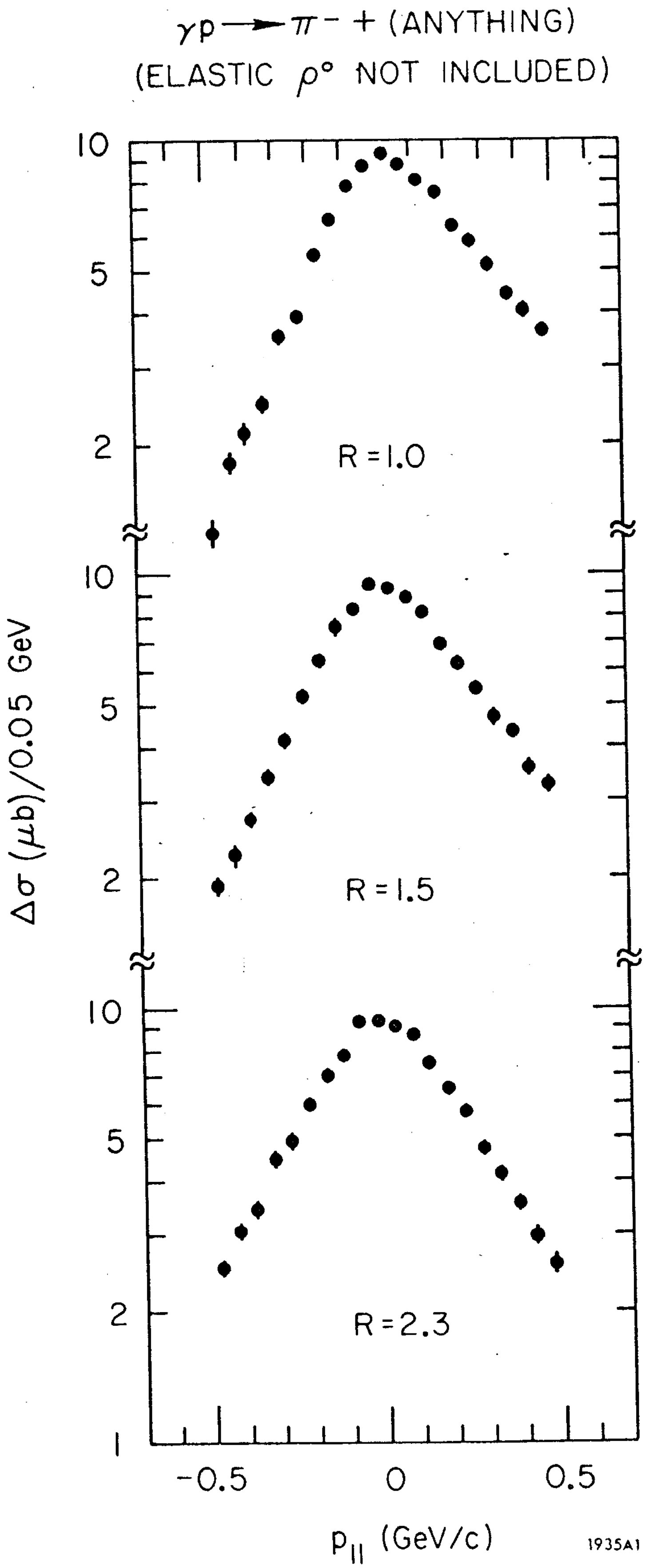

γp ⟶ π⁻ + (ANYTHING)
(ELASTIC ρ° NOT INCLUDED)
Δσ (μb)/0.05 GeV
10
5
2
R = 1.0
10
5
2
R = 1.5
10
5
2
R = 2.3
1
-0.5
0
0.5
p|| (GeV/c)
1935A1

Fig. 24